

THE DISCHARGE VARIABILITY OF NEOCORTICAL NEURONS DURING HIGH-CONDUCTANCE STATES

M. RUDOLPH* AND A. DESTEXHE

Unité de Neurosciences Intégratives et Computationnelles, CNRS, Bat. 32-33, Avenue de la Terrasse, 91198 Gif-sur-Yvette, France

Abstract—*In vivo* recordings have shown that the discharge of cortical neurons is often highly variable and can have statistics similar to a Poisson process with a coefficient of variation around unity. To investigate the determinants of this high variability, we analyzed the spontaneous discharge of Hodgkin-Huxley type models of cortical neurons, in which *in vivo*-like synaptic background activity was modeled by random release events at excitatory and inhibitory synapses. By using compartmental models with active dendrites, or single compartment models with fluctuating conductances and fluctuating currents, we found that a high discharge variability was always paralleled with a high-conductance state, while some active and passive cellular properties had only a minor impact. Furthermore, a balance between excitation and inhibition was not a necessary condition for high discharge variability. We conclude that the fluctuating high-conductance state caused by the ongoing activity in the cortical network *in vivo* may be viewed as a natural determinant of the highly variable discharges of these neurons. © 2003 IBRO. Published by Elsevier Science Ltd. All rights reserved.

Key words: cerebral cortex, computational models, coefficient of variation, Poisson process, conductance-based models.

Cortical neurons *in vivo* show a highly irregular discharge activity, both during sensory stimuli (e.g. Dean, 1981; Tolhurst et al., 1983; Softky and Koch, 1993; Holt et al., 1996; Shadlen and Newsome, 1998; Stevens and Zador, 1998; Shinomoto et al., 1999) and during spontaneous activity (e.g. Smith and Smith, 1965; Noda et al., 1970; Burns and Webb, 1976). The coefficient of variation (C_v), the standard measure for the variability of a spike train (see Experimental Procedures), was found to be higher than 0.5 for firing frequencies above 30 Hz in cat and macaque V1 and MT neurons (Softky and Koch, 1993). A C_v of 0.8 was reported as the lower limit under *in vivo* conditions by investigating the responses of individual MT neurons of alert macaque monkeys driven with constant-motion stimuli (Stevens and Zador, 1998).

*Corresponding author. Tel: +33-1-6982-4177; Fax: +33-1-6982-3427.

E-mail address: Michael.Rudolph@iaf.cnrs-gif.fr (M. Rudolph).

Abbreviations: AMPA, α -amino-3-hydroxy-5-methyl-4-isoxazolepropionic acid; C_v , coefficient of variation; EPSP, excitatory postsynaptic potential; IAF, integrate-and-fire; ISI, interspike interval; ISIH, interspike interval histogram; TTX, tetrodotoxin; V_m , membrane potential.

0306-4522/03/\$30.00+0.00 © 2003 IBRO. Published by Elsevier Science Ltd. All rights reserved.
doi:10.1016/S0306-4522(03)00164-7

Much theoretical work has since been devoted to find neuronal mechanisms responsible for the observed high firing irregularity. However, neither the integration of random excitatory postsynaptic potentials (EPSPs) by a simple leaky integrate-and-fire (IAF) neuron model, nor a more biophysical model of a layer V cell with passive dendrites were able to generate the high C_v observed *in vivo* (Softky and Koch, 1993). To solve this apparent discrepancy, balanced or “concurrent” inhibition and excitation was proposed as a mechanism producing a discharge activity with Poisson-type variability in IAF models (Shadlen and Newsome, 1994; Usher et al., 1994; Troyer and Miller, 1997; Shadlen and Newsome, 1998; Feng and Brown, 1998, 1999), or in single-compartment Hodgkin-Huxley type models (Bell et al., 1995). Later it was demonstrated that, using a leaky integrator model with partial reset mechanism or physiological gain, Poisson-distributed discharge activity at high frequencies can also be obtained without a fine tuning of inhibitory and excitatory inputs (Troyer and Miller, 1997; Christodoulou and Bugmann, 2000, 2001), indicating a possible role of nonlinear spike-generating dynamics for cortical spike-train statistics (Gutkin and Ermentrout, 1998). Recently, the “noisy” aspect of network dynamics was emphasized as a possible mechanism driving cortical neurons to fire irregularly (Usher et al., 1994; Hansel and Sompolinsky, 1996; Lin et al., 1998; Tiesinga and José, 1999). In this context, it was shown that (temporal) correlation in the inputs can produce a high C_v in the cellular response (Stevens and Zador, 1998; Sakai et al., 1999; Feng and Brown, 2000; Salinas and Sejnowski, 2000; for a review see Salinas and Sejnowski, 2001).

The consensus which emerged from these studies is that neurons operating in an excitable or noise-driven regime are capable of showing highly irregular responses. In this subthreshold regime, the membrane potential is close to spike threshold and action potentials are essentially triggered by fluctuations of the membrane potential. In this framework, the irregularity of the discharge and, thus, the C_v value, can be increased by either bringing the membrane closer to firing threshold (e.g. by balancing the mean of excitatory and inhibitory drive; see e.g. Bell et al., 1995; Shadlen and Newsome, 1998; Feng and Brown, 1998, 1999), or by increasing the noise amplitude (e.g. by correlating noisy synaptic inputs; see e.g. Feng and Brown, 2000; Salinas and Sejnowski, 2001). However, the conditions for the appearance of this subthreshold regime, as well as its dependence on various electrophysiological parameters or the characteristics of the driving inputs, are presently unclear.

The subthreshold regime of cortical neurons *in vivo* consists in large-amplitude voltage fluctuations (Matsumura et al., 1988; Contreras et al., 1996; Nowak et al., 1997; Paré et al., 1998; Azouz and Gray, 1999; Lampl et al., 1999). These fluctuations are caused by the high levels of spontaneous firing (from 5 to 20 Hz in awake animals; see Hubel, 1959; Evarts, 1964; Steriade, 1978; Matsumura et al., 1988; Holmes and Woody, 1989; Steriade et al., 2001) together with the dense interconnectivity of cortical neurons (several thousands of synaptic inputs per neuron; see Szentagothai, 1965; Cragg, 1967; Gruner et al., 1974; DeFelipe and Fariñas, 1992). In addition, this sustained synaptic activity is also responsible for setting cortical neurons into a high-conductance state (Borg-Graham et al., 1998; Paré et al., 1998), which is characterized by a depolarized membrane potential, as well as a reduced input resistance and time constant (Destexhe and Paré, 1999). However, although irregular firing activity was investigated in conductance-based models (e.g. Bell et al., 1995; Tiesinga and José, 1999; Salinas and Sejnowski, 2000; Tiesinga et al., 2000) the relation between high-conductance states and the highly irregular firing of cortical neurons has never been directly addressed.

In this paper we investigated the spike train statistics of spontaneously discharging non-bursting cortical neurons operating in a high-conductance state. To that end, we used both detailed multi-compartment models of morphologically reconstructed neocortical pyramidal neurons with active dendrites and a realistic representation of synaptic background activity, as well as simplified single-compartment models which include a two-conductance representation of background activity. Preliminary results have appeared in a conference paper (Rudolph and Destexhe, 2002).

EXPERIMENTAL PROCEDURES

Several types of conductance-based models of cortical neurons were considered.

Detailed biophysical model

Simulations were performed using a morphologically reconstructed neocortical pyramidal layer VI neuron of cat parietal cortex (Fig. 1A, Contreras et al., 1997). Passive model parameters were adjusted to intracellular recordings obtained after application of TTX and synaptic blockers (Destexhe and Paré, 1999) and kept constant over all simulations. An intracellular resistivity of $R_a=250 \Omega \text{ cm}^{-1}$, membrane resistivity of $R_m=22k \Omega \text{ cm}^2$ ($R_m=50 \Omega \text{ cm}^2$ in axon), and capacitance of $C_m=1 \mu\text{F cm}^{-2}$ ($C_m=0.04 \mu\text{F cm}^{-2}$ in axon) were used, where C_m was increased and R_m decreased by a factor of 1.45 to account for the surface correction due to dendritic spines, assuming that about 45% of the dendritic membrane area is represented by spines (DeFelipe and Fariñas, 1992).

Voltage-dependent conductances were inserted in the soma, dendrites and the axon (sodium current I_{Na} , delayed-rectifier potassium current I_{Kd} and voltage-dependent potassium current I_M). All currents were described by Hodgkin-Huxley type models (Hodgkin and Huxley, 1952) with kinetics taken from a model of hippocampal pyramidal cells (Traub and Miles, 1991), adjusted to match voltage-clamp data of cortical pyramidal cells (Huguenard et al., 1988). In the standard model,

constant peak conductance densities of 52.3 mS cm^{-2} (36.1 mS cm^{-2} in soma, 361 mS cm^{-2} in axon) for I_{Na} , 10.1 mS cm^{-2} (7 mS cm^{-2} in soma, 70 mS cm^{-2} in axon) for I_{Kd} , and 0.51 mS cm^{-2} (0.35 mS cm^{-2} in soma) for I_M (no I_M in axon) were used. These densities correspond to the values found experimentally in adult hippocampal pyramidal neurons (e.g. Magee and Johnston, 1995). To discuss the impact of membrane excitability, in some simulations the peak conductances of all ion channels were scaled by a common multiplicative factor. A “low” excitability (scale factor of 0.6, corresponding to the lower border of the experimental observed range) and a “high” excitability (scale factor of 1.4) deserved special attention.

To test the effects of active membrane properties, in some cases different sets of voltage-dependent conductances were used. This included Ca^{2+} -dependent potassium current (C-current) I_{KCa} (kinetics in Yamada et al., 1989; constant dendritic conductance density of 1 mS cm^{-2}), a high-threshold Ca^{2+} -current (L-current) I_{CaL} (kinetics in McCormick and Huguenard, 1992; conductance density of 3 mS cm^{-2} and 1.5 mS cm^{-2} for proximal and distal dendrites, respectively) and a persistent sodium current I_{NaP} (kinetics in French et al., 1990; Huguenard and McCormick, 1992; McCormick and Huguenard, 1992; constant dendritic conductance density of 0.1 mS cm^{-2}), as well as a model with different kinetics for I_{Na} , I_{Kd} and an A-type potassium current I_{KA} (Migliore et al., 1999).

Synaptic currents were incorporated using two-state kinetic models of glutamate α -amino-3-hydroxy-5-methyl-4-isoxazolepropionic acid (AMPA) and GABA_A receptor types (Destexhe et al., 1998) with quantal conductances of 869.4 pS (distal region, 600 pS for proximal region, see Fig. 1A) for AMPA and 1200 pS for GABA. These quantal conductances were estimated from miniature synaptic events (Destexhe and Paré, 1999). No metabotropic receptors were included. In some simulations, the quantal conductances were changed by a common factor to investigate the impact of the synaptic background strength. The densities of synapses in different regions of the layer VI cell under consideration were estimated from morphological studies in neocortical pyramidal cells (White, 1989; Larkman, 1991; DeFelipe and Fariñas, 1992), leading to a total of 16,563 glutamatergic and 3376 GABAergic synapses. To perform the simulations in a time-efficient manner, an accelerating algorithm (Lytton, 1996) was used.

Synaptic background activity was simulated by the random activity of inhibitory and excitatory synapses according to a Poisson process with average rates of $\nu_{inh}=5.5 \text{ Hz}$ for GABA_A synapses, and $\nu_{exc}=1.0 \text{ Hz}$ for AMPA synapses, as estimated from intracellular recordings of pyramidal neurons before and after application of TTX (Paré et al., 1998; Destexhe and Paré, 1999). In some simulations, the firing rates of inhibitory and excitatory synapses were changed. Such changes led to changes in the mean conductances underlying excitation and inhibition and, thus, allowed to shift the average membrane potential relative to firing threshold. Balanced or “concurrent” conditions refer to the situation where the mean inhibitory and excitatory conductances due to synaptic activity are such that the membrane operates close to firing threshold. Independent changes in the firing rate were used to investigate the cellular response in unbalanced conditions, i.e. in situations where the membrane is driven by either pronounced excitation or inhibition.

In addition to the firing rate, the statistics of the synaptic background activity was modified by introducing a correlation in the random background activity. To this end, N_0 independent random release events were redistributed among all N synapses, which for $N_0 < N$ leads to a co-release of several synapses, whereas every terminal still released according to a Poisson process (see details in Destexhe and Paré, 1999; Rudolph and Destexhe, 2001).

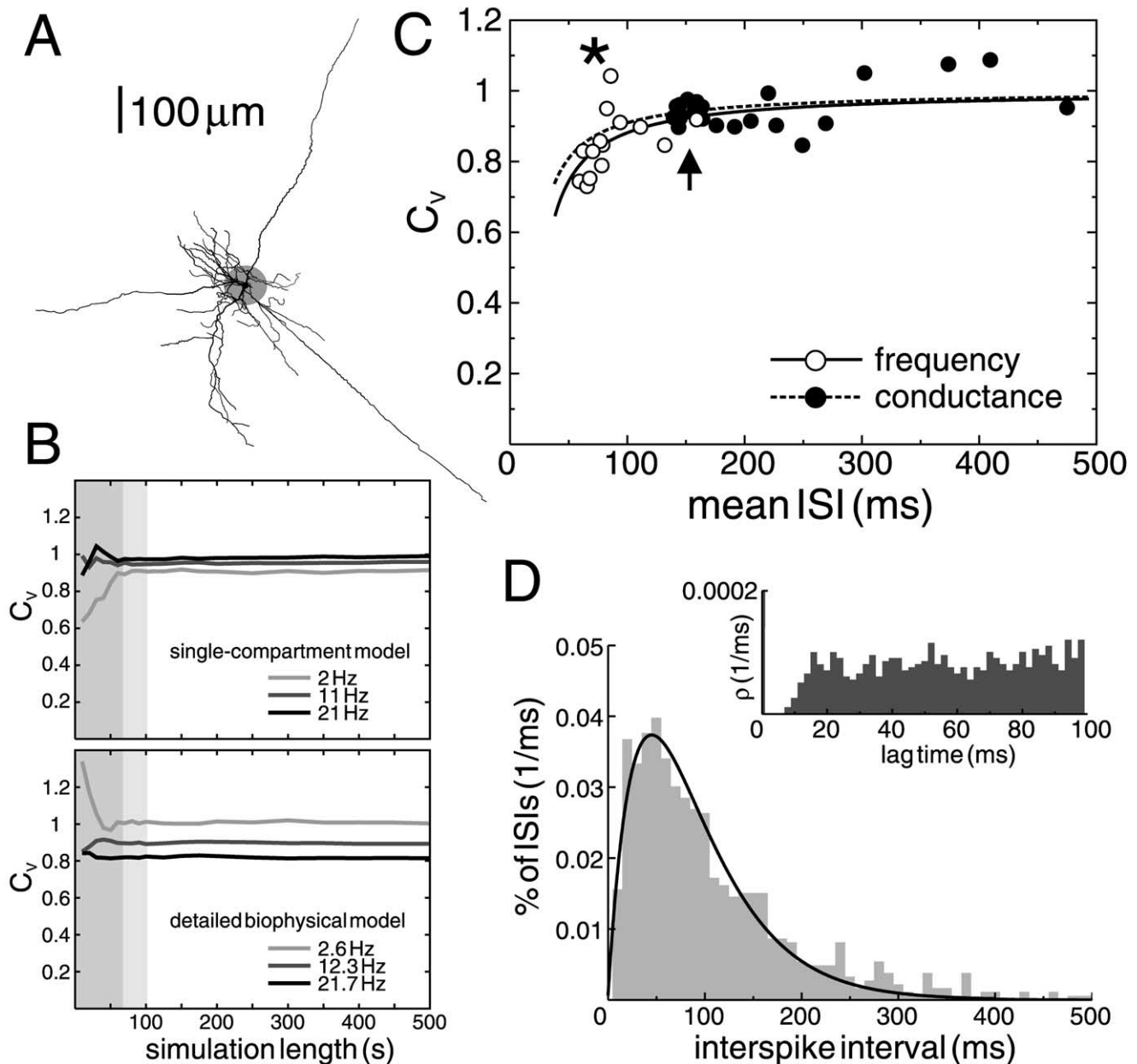


Fig. 1. Discharge variability in models of morphologically reconstructed cortical neurons. (A) Morphologically reconstructed neocortical pyramidal layer VI neuron of a cat incorporated in the models. The shaded area indicates the proximal region including all dendritic branches within a radius of 40 μm from the soma. Inside that region there were no excitatory synapses, whereas inhibitory synapses were spread over the whole dendritic tree. (B) Statistical validity of obtained results. The plots show the C_v as a function of the simulation length for representative examples of the simplified single-compartment model (top) and biophysical model (bottom) at different firing rates. Even for low firing rates (approximately 2 Hz), the C_v values deduced from the spontaneous discharge activity converged already after about 50 s to values obtained from marked extended simulation periods. The grey bars indicate the duration of the simulations used in the present study (see Experimental Procedures). (C) The C_v for spontaneous firing activity as a function of the mean ISI for different levels of background activity. The latter was altered either by a change in the quantal synaptic conductances, or the release frequency at excitatory and inhibitory synaptic terminals (ratio was kept constant) around the standard parameter setup (arrow, see Experimental Procedures). In both cases, correlated background activity with Pearson correlation coefficient of approximately 0.1 was used. The star refers to a spontaneous firing rate of about 15 Hz. Fits: Eq. 5 with $T_R=22$ mS for changes in frequency and $T_R=17$ ms for changes in quantal synaptic conductances. (D) Typical ISIH and autocorrelogram (inset) for the standard parameter setup with correlated background activity (Pearson correlation coefficient approximately 0.1) for a spontaneous firing rate of about 15 Hz (indicated by the star in B). Fit: Eq. 6 with $q=1$, $r=0.022$ ms^{-1} , $a=4.594$.

The impact of the cell morphology was addressed by using a simplified three-compartment model which had the same membrane area, input resistance and voltage attenuation as the layer

VI cell (Destexhe, 2001, see inset in Fig. 8A). The voltage-dependent currents I_{Na} , I_{Kd} and I_{M} used for the model had densities leading to an average membrane voltage V_m as well as V_m fluctuation

tuations corresponding to the low excitable model described above. The synaptic background activity (number of synapses, quantal conductances, release rates) was the same as in the detailed biophysical model.

Single-compartment models

Simplified models of synaptic background activity were constructed by incorporating Ornstein-Uhlenbeck processes (Uhlenbeck and Ornstein, 1930) into a single-compartment model with voltage-dependent currents I_{Na} , I_{Kd} and I_M corresponding to the detailed biophysical model. The time-dependent membrane current due to synaptic background activity $I_{syn}(t)$ was described by two different models. First, a *fluctuating conductance* model (see details in Destexhe et al., 2001), in which $I_{syn}(t)$ was decomposed into two time-dependent conductances (excitatory $g_e(t)$ and inhibitory $g_i(t)$), each described by one-variable stochastic process similar to the Ornstein-Uhlenbeck process:

$$I_{syn}(t) = g_e(t)(V(t) - E_e) + g_i(t)(V(t) - E_i) \quad (1)$$

$$\frac{dg_{i,e}(t)}{dt} = -\frac{1}{\tau_{i,e}}(g_{i,e}(t) - g_{i,0}) + \sqrt{D_{i,e}}W_{i,e} \quad (2)$$

where $g_{i,e,0}$ are average conductances, $\tau_{i,e}$ are time constants, $D_{i,e}$ are noise diffusion coefficients, and $W_{i,e}$ denotes Gaussian white noise of unit S.D. and zero mean for inhibition and excitation, respectively. White noise is obtained for $\tau_{i,e} = 0$, and $\tau_{i,e} > 0$ yields “colored” noise. The relation between $D_{i,e}$ and the S.D. $\sigma_{i,e}$ of the variables $g_{i,e}(t)$ is given by $\sigma_{i,e}^2 = \frac{1}{2} D_{i,e} \tau_{i,e}$ (see Gillespie, 1996). Typical parameter values are $E_e = 0$ mV, $E_i = -75$ mV, $g_{e0} = 0.0121$ μ S, $g_{i0} = 0.0573$ μ S, $\sigma_e = 0.025$ μ S, $\sigma_i = 2.5$ σ_e , $\tau_e = 10.49$ ms, $\tau_i = 2.728$ ms.

The second model used was a *fluctuating current* model, where $I_{syn}(t)$ was directly described by an one-variable Ornstein-Uhlenbeck process without the involvement of conductances:

$$\frac{dI_{syn}(t)}{dt} = -\frac{1}{\tau_{syn}}(I_{syn}(t) - I_{syn0}) + \sqrt{D_{I_{syn}}}W_{I_{syn}} \quad (3)$$

where $\sigma_{I_{syn}}^2 = \frac{1}{2} D_{I_{syn}} \tau_{syn}$ (see e.g. Tiesinga et al., 2000; Brunel et al., 2001). Typical parameter values are $I_{syn0} = -0.4$ nA, $\sigma_{I_{syn}} = 0.4$ nA, $\tau_{I_{syn}} = 2$ ms. In addition, two further variations of these models were used. In one case there was a static (DC) conductance with current fluctuations (typical parameter values: $E_e = 0$ mV, $E_i = -75$ mV, $g_{e0} = 0.0121$ μ S, $g_{i0} = 0.0573$ μ S, $\sigma_{I_{syn}} = 1.0$ nA, $\tau_{I_{syn}} = 2$ ms), and in another case there was a static (DC) current added to fluctuating conductances (typical parameter values: $I_{syn0} = -0.33$ nA, $E_e = 0$ mV, $E_i = -75$ mV, $\sigma_e = 0.012$ μ S, $\sigma_i = 0.0264$ μ S, $\tau_e = 10.49$ ms, $\tau_i = 2.728$ ms).

All simulations were performed using the NEURON simulation environment (Hines and Carnevale, 1997), running on DELL computers (Dell Computer Corporation, Round Rock, TX, USA) under the LINUX operating system.

Data acquisition and analysis

Records of spike-release events at the soma with a temporal precision of 0.1 ms from simulation lasting 60 s–100 s for each parameter set constitute the data basis for the present investigation. In most cases, the coefficient of variation C_v , defined by the ratio between the S.D. and mean of the interspike intervals (ISIs)

$$C_v = \frac{\text{S.D. of ISIs}}{\text{mean ISI}} \quad (4)$$

could be deduced with reliable statistics. The statistical validity of the results was addressed by running simulations of up to 1000 s duration for representative parameter sets in both simplified single-compartment models and detailed multi-compartment models. Analyzing the C_v as a function of the simulation length showed

that in all cases even at low firing rates (approximately 2 Hz), the C_v values deduced from the spontaneous-discharge activity converged already after about 50 s to values obtained from marked extended simulation periods (see Fig. 1B).

For a Poisson process with refractory period T_R , the C_v only depends on the mean ISI and T_R (see e.g. Bugmann, 1995; Christodoulou and Bugmann, 2001):

$$C_v = \sqrt{\frac{\text{mean ISI} - T_R}{\text{mean ISI}}} \quad (5)$$

To investigate the impact of a specific model parameter, simulations were performed by changing the parameter in question while keeping all other fixed. In general, these changes were accompanied by changes in the firing rate, and allowed to depict the C_v as a function of the mean ISI. For a given data set, the C_v as a function of the mean ISI was fitted using Eq. 5 with T_R as a free parameter. The T_R which yielded the best fit can be viewed as characterizing the “effective” refractoriness of the Poisson trains produced by the model. This effective refractory period is expected to depend on both cellular properties (channel kinetics, membrane excitability, passive membrane properties) as well as the characteristics of the driving synaptic background activity and, thus, will be different for different data sets.

To investigate if the recorded spike train resembles that of a Poisson-type firing process, the ISIs were analyzed for exponential distribution. To that end, ISI histograms (ISIH) were constructed and fitted by gamma distributions

$$p_{\text{ISI}}(T) = \frac{ar(rT)^{a-1} \exp(-rT)}{q!} \quad (6)$$

where $p_{\text{ISI}}(T)$ denotes the probability for occurrence of ISIs of length T and r , a and q are parameters. In addition, autocorrelograms (displaying the probability ρ) of the output spike trains were constructed to show independence of the spike events.

In order to link the subthreshold dynamics to the firing activity, we investigated the C_v and the mean ISI as a function of the following measure of proximity to firing threshold

$$\Delta = \frac{\sigma_v}{V_T - \bar{V}} \quad (7)$$

where σ_v denotes the S.D. of membrane potential fluctuations, \bar{V} the mean membrane potential and V_T the mean firing threshold. In all cases, σ_v and \bar{V} were estimated from voltage traces from which spikes were removed. Unless otherwise stated, a mean firing threshold V_T of -50 mV was used. The latter was estimated from the models and showed little (< 1 mV) variations for changes in the parameters considered here. Δ can be viewed as an “effective” inverse distance to firing threshold and will be referred to as “threshold accessibility”. Higher values of Δ correspond to an activity closer to threshold, either caused by a larger fluctuation amplitude σ_v or a reduced distance between the average membrane potential \bar{V} and the firing threshold V_T .

RESULTS

High discharge variability in the detailed biophysical model

We first used a compartmental model of a neocortical pyramidal neuron with active dendrites (see Experimental Procedures). This model was constrained from *in vivo* intracellular measurements of the impact of background activity (Paré et al., 1998; Destexhe and Paré, 1999). In agreement with *in vivo* recordings, the model displayed a depolarized V_m , high-frequency V_m fluctuations and a marked decrease of input resistance (high-conductance

state), which markedly impacted the cell's responsiveness (see e.g. Hô and Destexhe, 2000). The cell also displayed a spontaneous discharge activity with rates between 5 and 20 Hz, in agreement with recordings of cortical neurons in awake animals (Hubel, 1959; Evarts, 1964; Steriade, 1978; Matsumura et al., 1988; Holmes and Woody, 1989; Steriade et al., 2001).

To quantify the variability of these spontaneous discharge patterns, the C_V was calculated for models with various cellular and background properties. In a first series of simulations, we altered the strength of the background activity by changing either the synaptic release rates (keeping the v_{inh}/v_{exc} ratio fixed), or the quantal conductances of AMPA and GABA_A receptors. In both cases, the output spike train showed a high variability, quantified by a C_V between 0.8 and 1.0 (Fig. 1C). Increasing the quantal conductances from 50% to 200% of the standard values (see Experimental Procedures; Fig. 1C, arrow) led to an increase in the cell's firing rate from 0.2 to 8 Hz; further increases in quantal conductance did not further increase the cell's firing rate. For a similar relative change in the release rates, the firing rate varied between 7 and 20 Hz. This result can be explained by pointing to the tight relation between intracellular V_m fluctuations, quantified by the S.D. σ_V , and the spiking response. The increase in the synaptic release frequency of both excitation and inhibition only minimally changed σ_V between 3.5 and 4 mV. The membrane's threshold accessibility Δ changed only minimally, with higher frequencies leading to a shift towards the firing threshold (increase in Δ) and shorter mean ISIs (see Fig. 2A, white dots). This indicates a stable balance between inhibition and excitation. In contrast, for changes in the quantal conductances, the σ_V increased from 1.9 mV to about 4 mV, reflecting in a larger effective shift towards firing threshold in the investigated parameter range (Fig. 2A, black dots). In both cases we observed a saturation in the fluctuation amplitude, meaning that no further increase in σ_V and, thus, the firing rate could be obtained even for very high synaptic conductances or release rates. Therefore a C_V for lower mean ISIs could not be deduced. However, fits of the available data show that in all cases the output spike trains resemble Poisson trains. This conclusion is further supported by ISI histograms and autocorrelograms (Fig. 1D), which show that these spike trains are both exponentially distributed according to a gamma distribution and independent.

In a second series of simulations we addressed the effect of the statistical properties of background activity on the variability of discharges. To this end, we altered the correlation among the spatially distributed synapses. An increase in the correlation (between 0 and 0.3 Pearson's correlation coefficient) led to a marked increase in σ_V (between 1.5 and 6.5 mV for the standard model) and, thus, an effective shift towards firing threshold (Fig. 2B). This shift was accompanied by an increase in the firing rate (between 0 and 50 Hz for the standard model) for all investigated membrane excitabilities. Surprisingly, despite the differences in the threshold accessibility Δ , the output spike trains showed a high irregularity with C_V values

between 0.8 and 1.0 (Figs. 3A and 2B) with exponentially distributed and independent ISIs (for a representative example see Fig. 1D), resembling the behavior expected from a Poisson process with refractory period. This suggests that, under physiological conditions, the appearance of highly irregular discharge patterns only weakly depends on the effective distance to firing threshold and, thus, the operating point in the subthreshold regime.

Interestingly, for comparable mean ISIs, the effective distance to firing threshold was smaller (larger Δ) for the standard setup (see Fig. 2B, right, black triangles). For higher excitable membranes, the higher membrane conductance shifts the average membrane potential towards the leak reversal potential. In addition, in more excitable membranes, smaller membrane potential fluctuations are needed to elicit spikes. Both effects together yield, compared to models with lower excitability, smaller Δ values for evoking spontaneous discharges at a given frequency (Fig. 2B, compare white dots with black triangles). On the other hand, if the membrane excitability is too low (Fig. 2B, black dots), the overall smaller membrane conductance brings the average membrane potential closer to threshold, whereas higher fluctuations are needed in order to elicit spikes at a given frequency. Both opposing effects yield an effective distance to threshold which was, for a given mean ISI, slightly larger (smaller Δ) than that for models with higher membrane excitability (Fig. 2B, compare black dots with black triangles).

We further investigated the impact of the membrane excitability on the effective distance to threshold and its role in modulating the variability of discharges by scaling the ion channel densities (see Experimental Procedures) for fixed background activity. An increase in the overall membrane excitability had a major impact on the average firing rate displayed by the cell, but not on the C_V (Fig. 3A). For a broad range of membrane excitabilities, between 80% and 200% around the standard values, the C_V was about 0.8 for firing rates up to 20 Hz (Fig. 3B). When the membrane excitability was less than 80% of the standard value, the firing rate was too low (<0.2 Hz) for obtaining statistically reliable estimates of the C_V . As mentioned above, there was only a weak relation between the irregularity of the discharge and the threshold accessibility Δ and, thus, the membrane excitability (Fig. 2C, left). However, for increasing excitability, which was accompanied by a decrease in the mean ISI, Δ increased (Fig. 2C, right), indicating an effective shift towards firing threshold. For a further increase in the membrane excitability and mean firing rate, the opposite was seen, namely an increase in the distance (decrease in Δ , Fig. 2C, right). This suggests that for an intermediate excitability, the opposing effects of increased membrane potential fluctuations due to higher excitability and the shift towards the resting potential due to an increase in the overall membrane conductance at higher excitability counterbalance. The latter results in an effective shift towards the firing threshold but had no obvious impact on the discharge irregularity.

We also tested the dependence of the variability of the kinetics and the type of ion channels present in the mem-

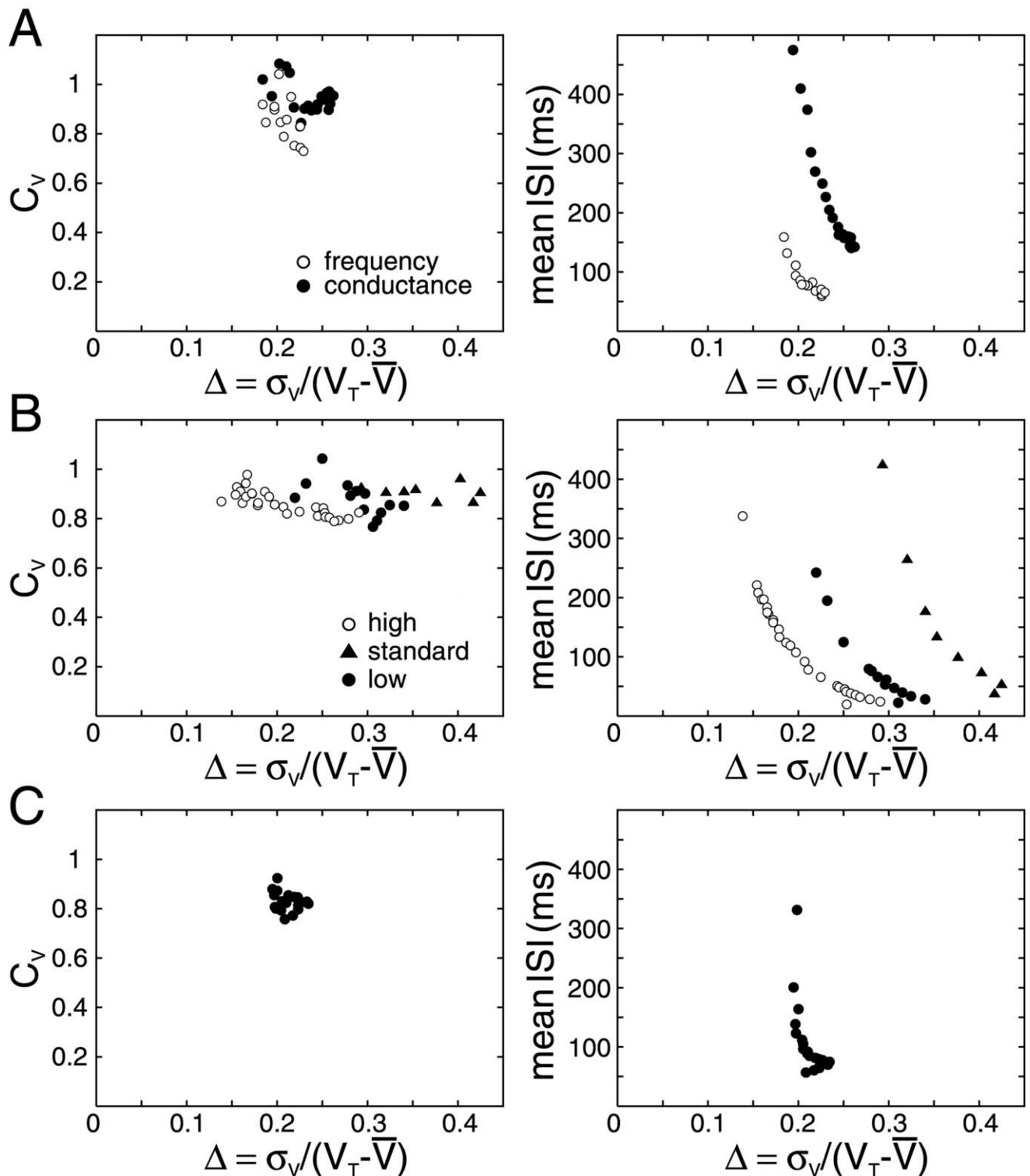


Fig. 2. Characterization of discharge activity as a function of the threshold accessibility. The C_v (left) and the mean ISI (right) are shown as functions of Δ , defined as the ratio between the membrane potential fluctuation amplitude σ_v and the distance between the firing threshold V_T , fixed to -50 mV in all cases, and the mean membrane potential \bar{V} (Eq. 7). (A) Results for different levels of background activity, obtained either by a change in the quantal synaptic conductances, or the release frequency at excitatory and inhibitory synaptic terminals (ratio was kept constant) around the standard parameter setup (see Experimental Procedures). The data correspond to the one shown in Fig. 1C. (B) Results for the high and low excitable as well as the standard model (see Experimental Procedures). The firing rate was changed by altering the correlation in the synaptic background activity. (C) Results for different levels of membrane excitability in the presence of correlated background activity (Pearson correlation coefficient of approximately 0.1).

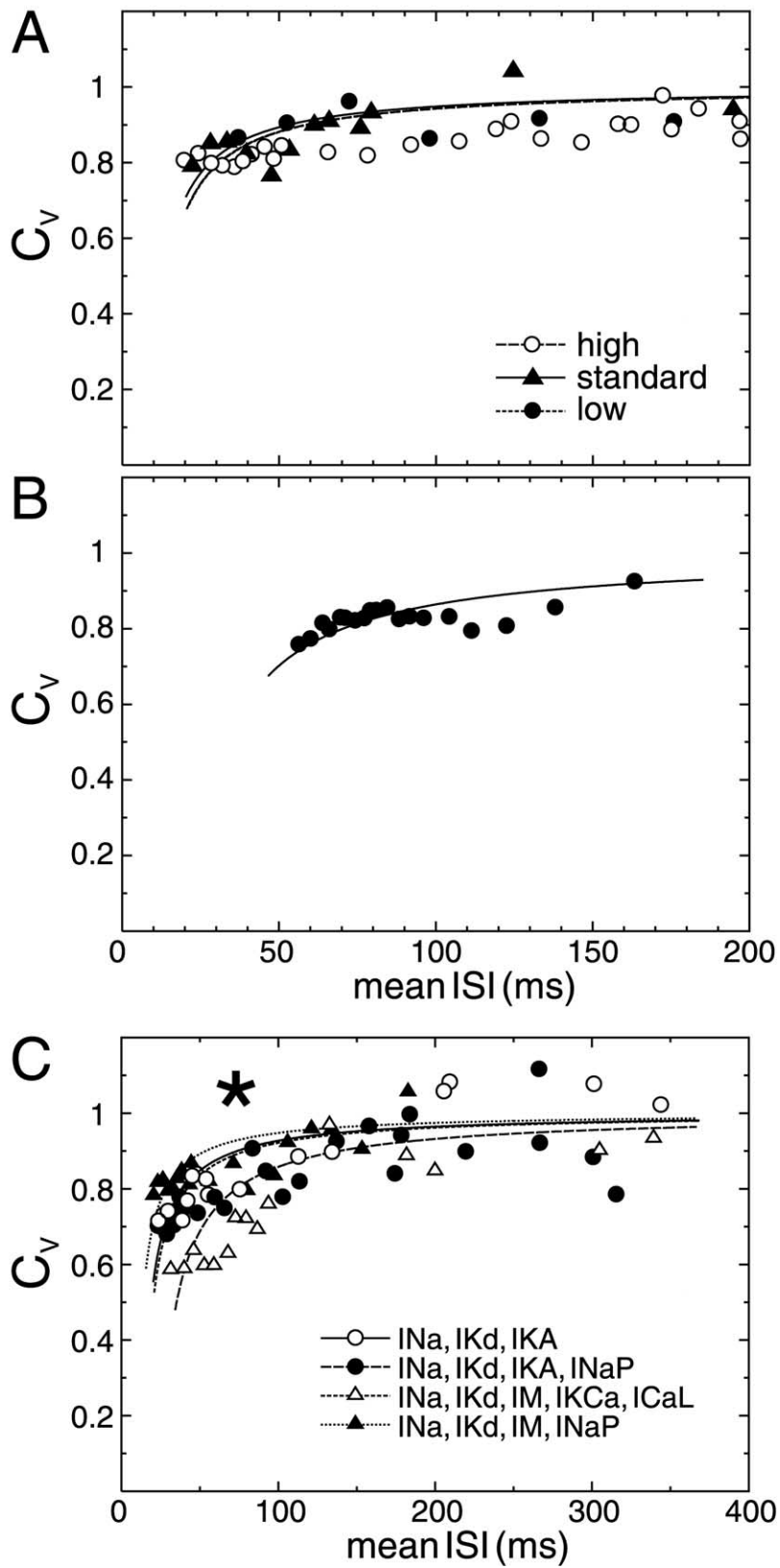


Fig. 3. (Caption overleaf).

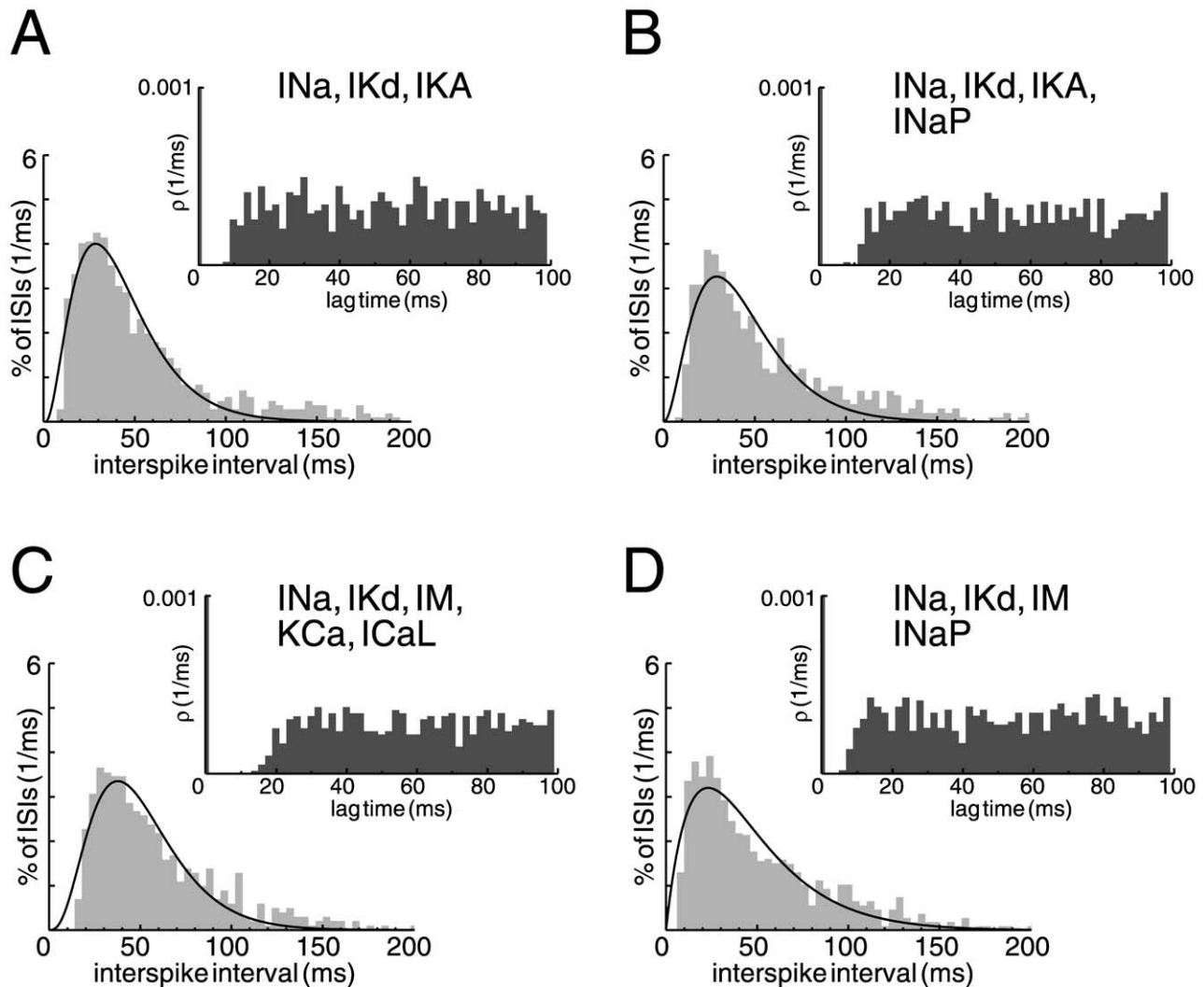


Fig. 4. Typical ISI histograms and autocorrelograms (insets) for various ion-channel settings (see Fig. 3C). (A) Voltage-dependent conductances including sodium I_{Na} and delayed-rectifier potassium channels I_{Kd} as well as A-type potassium channels I_{KA} according to (Migliore et al., 1999). Fit: Eq. 6 with $q=2$, $r=0.073 \text{ ms}^{-1}$, $a=2.012$. (B) Settings as in A with additional persistent sodium current I_{NaP} (French et al., 1990; Huguenard and McCormick, 1992; McCormick and Huguenard, 1992). Fit: Eq. 6 with $q=2$, $r=0.069 \text{ ms}^{-1}$, $a=1.744$. (C) I_{Na} , I_{Kd} and I_M (standard model, see Experimental Procedures) with additional Ca^{2+} -dependent potassium current (C-current) I_{KCa} (Yamada et al., 1989) and a high-threshold Ca^{2+} -current (L-current) I_{CaL} (McCormick and Huguenard, 1992). Fit: Eq. 6 with $q=3$, $r=0.079 \text{ ms}^{-1}$, $a=1.869$. (D) I_{Na} , I_{Kd} and I_M (standard model, see Experimental Procedures) with additional persistent sodium current I_{NaP} . For more details see Experimental Procedures. All plots were obtained for a spontaneous activity at about 15 Hz firing rate (see star in Fig. 3C). Fit: Eq. 6 with $q=1$, $r=0.043 \text{ ms}^{-1}$, $a=2.004$.

brane. As shown in Fig. 3C, the C_V was always between 0.8 and 1.2 for spontaneous firing frequencies lower than

10 Hz. Fits to the C_V as a function of the mean ISI (curves in Fig. 3C) as well as the ISI histograms (Fig. 4) along with

Fig. 3. High variability of discharge for various ion channel settings. (A) The C_V as a function of the mean ISI for the high and low excitable as well as the standard model (see Experimental Procedures). The firing rate was changed by altering the correlation in the synaptic background activity. Fits: Eq. 5 with $T_R=11.1 \text{ ms}$ for high, $T_R=10.1 \text{ ms}$ for mid and $T_R=11.2 \text{ ms}$ for low excitability. Corresponding plots with the C_V and mean ISI as functions of the threshold accessibility are shown in Fig. 2B. (B) C_V versus mean ISI for different levels of membrane excitability in the presence of correlated background activity (Pearson correlation coefficient of approximately 0.1). Fit: Eq. 5 with $T_R=25.4 \text{ ms}$. Corresponding plots showing the C_V and mean ISI as functions of the threshold accessibility are presented in Fig. 2C. (C) The variability as a function of mean ISI for various ion channel settings and kinetics. White dots: voltage-dependent conductances including sodium I_{Na} and delayed-rectifier potassium channels I_{Kd} as well as A-type potassium channels I_{KA} , according to Migliore et al. (1999). Fit: Eq. 5 with $T_R=14.0 \text{ ms}$. Black dots: I_{Na} , I_{Kd} and I_{KA} conductances (Migliore et al., 1999) with additional persistent sodium current I_{NaP} (French et al., 1990; Huguenard and McCormick, 1992; McCormick and Huguenard, 1992). Fit: Eq. 5 with $T_R=15.1 \text{ ms}$. White triangles: I_{Na} , I_{Kd} and I_M (standard parameter setup, see Experimental Procedures) with additional Ca^{2+} -dependent potassium current (C-current) I_{KCa} (Yamada et al., 1989) and a high-threshold Ca^{2+} -current (L-current) I_{CaL} (McCormick and Huguenard, 1992). Fit: Eq. 5 with $T_R=26.4 \text{ ms}$. Black triangles: I_{Na} , I_{Kd} and I_M (standard parameter setup, see Experimental Procedures) with additional persistent sodium current I_{NaP} . Fit: Eq. 5 with $T_R=10.2 \text{ ms}$. The star refers to a spontaneous firing rate of about 15 Hz. For more details, see Experimental Procedures.

the flat autocorrelograms indicate that in all cases the spiking activity can be well described by a Poisson process with refractory period. Changes in the membrane time constant due to different ion channels directly translated into a change in the effective refractory period and, this way, a shift of the fitting curves. Representative ISIHs and autocorrelograms (spontaneous firing rate of 15 Hz, see star in Fig. 3C) for all cases are shown in Fig. 4. The histograms are well fit by gamma distributions, and the autocorrelograms are flat except for intervals shorter than the refractory period, supporting the conclusion that the output spike pattern resembles that of a nearly ideal Poisson process.

The threshold accessibility Δ covered a broad range of values, with an increase in Δ yielding a decrease in the mean ISIs (Fig. 5B, right) and a slight decrease in the C_v (Fig. 5B, left) for all investigated active conductance settings. The latter decrease must be viewed as a direct result of the higher discharge rate, which is accompanied by the membrane operating closer to firing threshold (thus yielding larger Δ), but also limits the irregularity of the discharge due to the impact of the refractory period. Taken together, the obtained results allow the conclusion that within the limits of the investigated parameter spectrum, the exact nature of the spike-generating mechanisms, the channel kinetics and channel distributions showed only minor effects on the Poisson structure of the spontaneous discharge and its firing variability.

Balanced inhibition and excitation was proposed as a possible mechanism for the high variability of cortical neuron discharges (Shadlen and Newsome, 1994; Bell et al., 1995; Feng and Brown, 1998, 1999, 2000; but see König et al., 1996). In order to test this hypothesis, we independently changed the excitatory and inhibitory release rates (ν_{exc} and ν_{inh} , respectively) within some range around their experimentally constrained mean values (see Experimental Procedures; Fig. 6A: 50%–300% and 70%–150% for excitation and inhibition, respectively). Such changes in the release rates shifted the average membrane potential relative to firing threshold due to changes in the mean inhibitory and excitatory synaptic conductances (see Fig. 5A). Here, diminishing inhibition or pronouncing excitation yielded a decrease in the effective distance to firing threshold (increase in Δ), which was accompanied by an increase in the firing rate (decrease in the mean ISI, see Fig. 5A, right) as well as a decrease in the discharge variability (Fig. 5A, left) due to the impact of the refractory period. However, for synaptic background activity determined to an increasing extent by excitation, Δ decreased after passing a maximal value. Given the fact that changes in the firing rate at synaptic terminals directly impact the total membrane conductance, the appearance of such a maximum is comparable to the situation we encountered for variable membrane excitability (see Fig. 2C): although a higher activity at synaptic terminals increases the membrane-potential fluctuation amplitude (thus yielding an increase in Δ), the increase in the overall membrane conductance accompanying a pronounced synaptic activity effectively diminishes V_m fluctuations and shifts the aver-

age membrane potential towards the leak-reversal potential (thus yielding an decrease in Δ). Both effects counterbalance, resulting in a condition where the average membrane potential comes closest to the threshold for eliciting spikes.

Below 50 Hz, the variations of the C_v as a function of the release rates (Fig. 6A) was entirely an effect of firing-rate modulation (Fig. 6B). There was a clear deviation from Poisson-type firing at higher firing frequencies (Fig. 6B, left star), which occurred when combining strong excitation with weak inhibition. In this case, the autocorrelograms deviated from a flat shape (Fig. 6C inset), which was due to a tendency to produce bursts of spikes (mostly doublets) with an ISI of about 8 ms, the typical membrane refractory period. This indicates that the cell, driven by the excitatory background, fires in a sustained way with high rates only constrained by the refractory period. On the other hand, for most of the cases, the firing rate was below 50 Hz and the corresponding C_v was larger than 0.5 (Fig. 6B). In those cases, the ISIs were exponentially distributed (Fig. 6D). This behavior was present even for large disturbances in the release rates of excitation and inhibition, suggesting that the “balance” hypothesis does not apply to this model.

To further probe the impact of the balance between excitation and inhibition, we varied the excitatory release rate while keeping the inhibitory release rate constant. Fig. 7A shows that the C_v was always high for all investigated unbalanced conditions. The Poisson structure of the output spike train depended on the statistics of the background activity. For low correlations, the deviation from the exponential distribution (Fig. 7B) was larger than for high correlations (Fig. 7C; both cases are for ν_{exc} approximately 2 Hz, see star in Fig. 7A).

These results argue for an impact of the morphology on the output spike pattern: with increasing correlation, spatially distributed synaptic inputs become more synchronized, thus diminishing the role of the location of an individual synaptic stimulation. To investigate this further, we abstracted from the cell's morphological structure by collapsing the dendritic tree into three compartments of same total membrane area, representing the perisomatic, proximal and distal regions (Fig. 8A, inset; see details in Experimental Procedures). Interestingly, the variability of the spiking output was slightly higher than in the detailed model (above 0.9 for firing rates below 50 Hz, see Fig. 8A), but showed only a minor dependence on the strength of the synaptic background activity. The latter was changed by scaling all quantal conductances with a common factor. A lower refractory period compared to the detailed model could be deduced from the fitting curves, indicating that membrane properties responsible for the refractory period do have a less effective impact in the case of a simplified morphology (compare with Fig. 3A). ISIH and autocorrelograms indicate only a slight deviation from the behavior expected from an ideal gamma distribution and independent Poisson process (Fig. 8B).

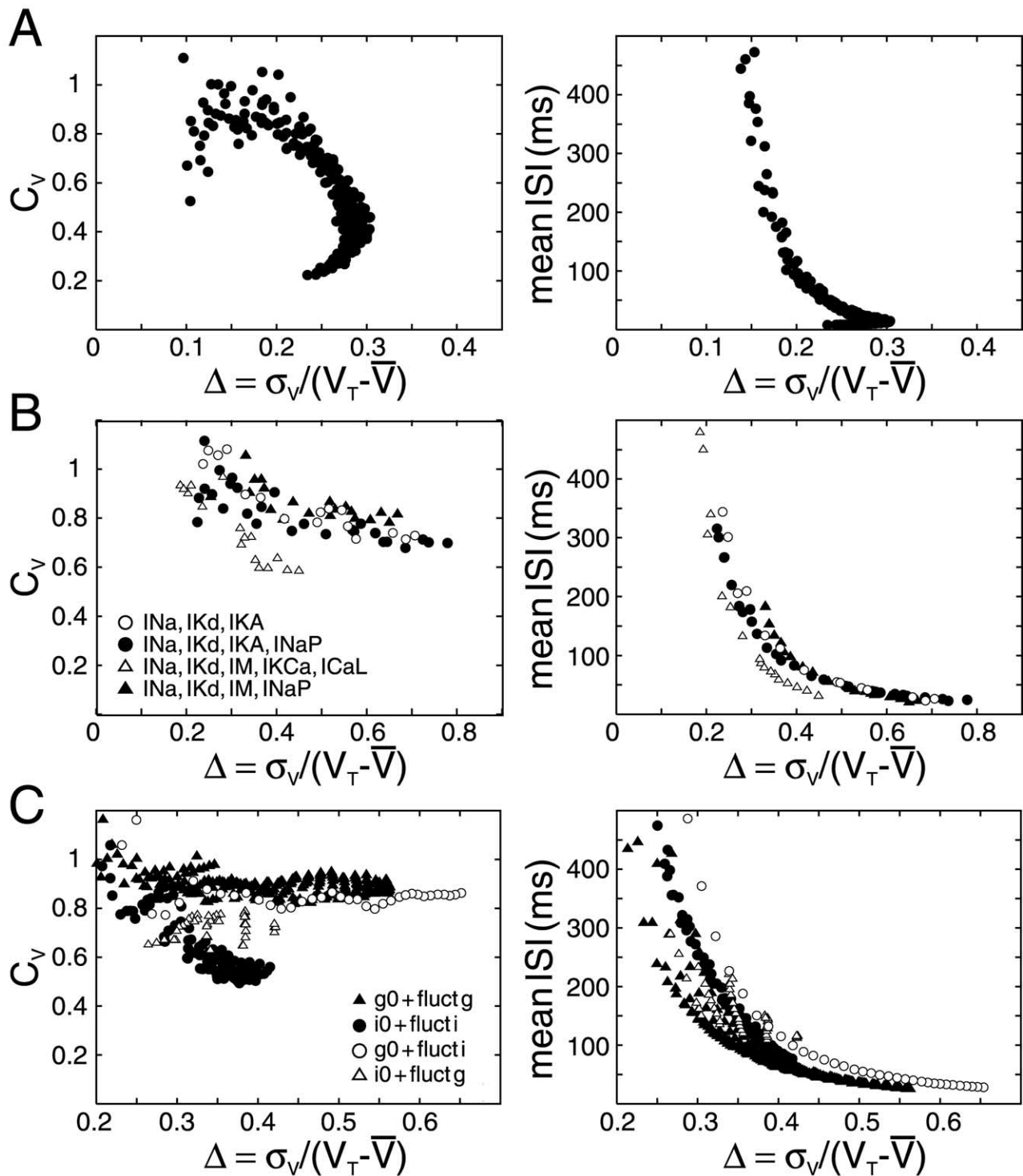


Fig. 5. Characterization of discharge activity as a function of the threshold accessibility. The C_v (left) and the mean ISI (right) are shown as functions of Δ , defined as the ratio between the membrane-potential fluctuation amplitude σ_v and the distance between the firing threshold V_T , fixed to -50 mV in all cases (except for the setup with Ca^{2+} currents in B, where $V_T = -44.5$ mV), and the mean membrane potential \bar{V} (Eq. 7). (A) Results for different excitatory frequencies (scaled between 50% and 300% around the experimentally determined mean value of 1 Hz) and inhibitory frequencies ν_{inh} (scaled between 70% and 150% around the experimentally determined mean value of 5.5 Hz). (B) Results for various ion channel settings and kinetics. The data and setups correspond to Fig. 3C. (C) Results for various simplified models of synaptic background activity: a point-conductance model ($g_0 + \text{fluct } g$), a fluctuating current model ($i_0 + \text{fluct } i$), a model using a constant current with fluctuating conductance around zero mean ($i_0 + \text{fluct } g$) and a model using a constant conductance with fluctuating current around zero mean ($g_0 + \text{fluct } i$). Model parameters were for $g_0 + \text{fluct } g$: $g_{e0} = 0.0121 \mu\text{S}$, $g_{i0} = 0.0573 \mu\text{S}$, $0.003 \mu\text{S} \leq \sigma_e \leq 0.035 \mu\text{S}$, $0.006 \mu\text{S} \leq \sigma_i < 0.07 \mu\text{S}$; for $i_0 + \text{fluct } i$: $-0.46 \text{ nA} \leq I_{\text{syn}0} \leq -0.34 \text{ nA}$, $0.05 \text{ nA} \leq \sigma_{\text{isyn}} \leq 2.0 \text{ nA}$; for $i_0 + \text{fluct } g$: $I_{\text{syn}0} = -0.34 \text{ nA}$, $0.002 \mu\text{S} \leq \sigma_e \leq 0.03 \mu\text{S}$, $0 \mu\text{S} \leq \sigma_i \leq 0.08 \mu\text{S}$; for $g_0 + \text{fluct } i$: $g_{e0} = 0.0121 \mu\text{S}$, $g_{i0} = 0.0573 \mu\text{S}$, $0.5 \text{ nA} \leq \sigma_{\text{isyn}} \leq 2.5 \text{ nA}$.

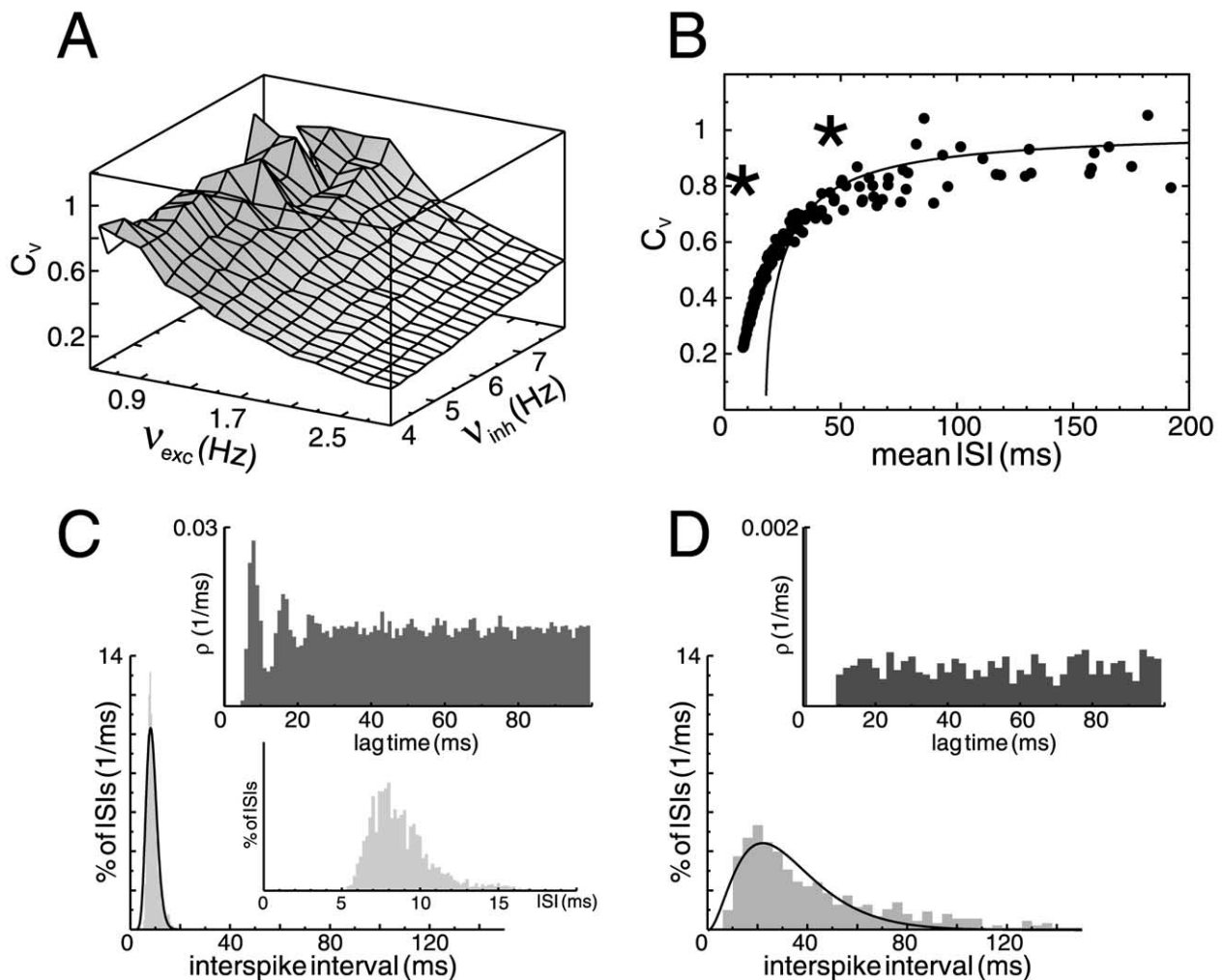


Fig. 6. The impact of concurrent inhibition and excitation on the firing variability. (A) The C_V as a function of excitatory frequency v_{exc} (scaled between 50% and 300% around the experimentally constrained mean value of 1 Hz) and inhibitory frequency v_{inh} (scaled between 70% and 150% around the experimentally determined mean value of 5.5 Hz). (B) C_V values from A depicted as a function of the mean ISI. The data show a clear deviation from Poisson-like firing at very high firing rates (mean ISI < 20 ms). The left star indicates deviation from Poisson type firing at firing frequencies above 100 Hz, the right star indicates a spontaneous firing rate of about 23 Hz. Fit: Eq. 5 with $T_R=17.8$ ms. Corresponding plots with the C_V and mean ISI as functions of the threshold accessibility are shown in Fig. 5A. (C) and (D). ISH and autocorrelograms (insets) for $v_{exc}=2.7$ Hz, $v_{inh}=4.4$ Hz (C) and $v_{exc}=1.1$ Hz, $v_{inh}=4.4$ Hz (D). Whereas in the case of strong excitation the sustained high firing rate around 110 Hz (indicated by left star in B) causes a clear correlation between ISIs (peaks in the autocorrelogram in (C), inset) and, thus, a deviation from Poisson-type firing, at smaller firing rates around 23 Hz (indicated by right star in B) the cell returns to Poisson-like firing patterns (D). All results are from models with high membrane excitability (see Experimental Procedures) and correlated background activity (Pearson correlation coefficient approximately 0.1). Fits: Eq. 6 with $q=15$, $r=1.848$ ms $^{-1}$, $a=0.544$ (C) and $q=2$, $r=0.091$ ms $^{-1}$, $a=1.805$ (D).

Simplified models of cortical neurons and discharge variability

The results obtained with the three-compartment model point towards a limit in reducing the morphology of the cell while keeping the same number of randomly releasing synapses. We therefore investigated another type of approach, in which background activity was represented by two fluctuating conductances, which parameters can be adjusted to reproduce the statistical properties of conductance and voltage fluctuations due to background activity (Destexhe et al., 2001). This point-conductance model consists of two conductances, excitatory and inhibitory, which vary according to a stochastic (Ornstein-Uhlenbeck)

process (see Experimental Procedures). Including this point-conductance model in a single-compartment Hodgkin-Huxley neuron, or in real cortical neurons *in vitro*, can lead to *in vivo*-like characteristics, such as a high discharge variability (Destexhe et al., 2001).

Two of the parameters of this model, the mean excitatory and inhibitory conductances (g_{e0} and g_{i0}), are best suited to probe the role of the excitatory–inhibitory balance on discharge variability. When varying these parameters, the spontaneous spike trains showed a high variability described by a C_V above 0.6 (Fig. 9A) in the whole investigated range (between 20% and 250% around the standard values for both g_{e0} and g_{i0}). This result compares to

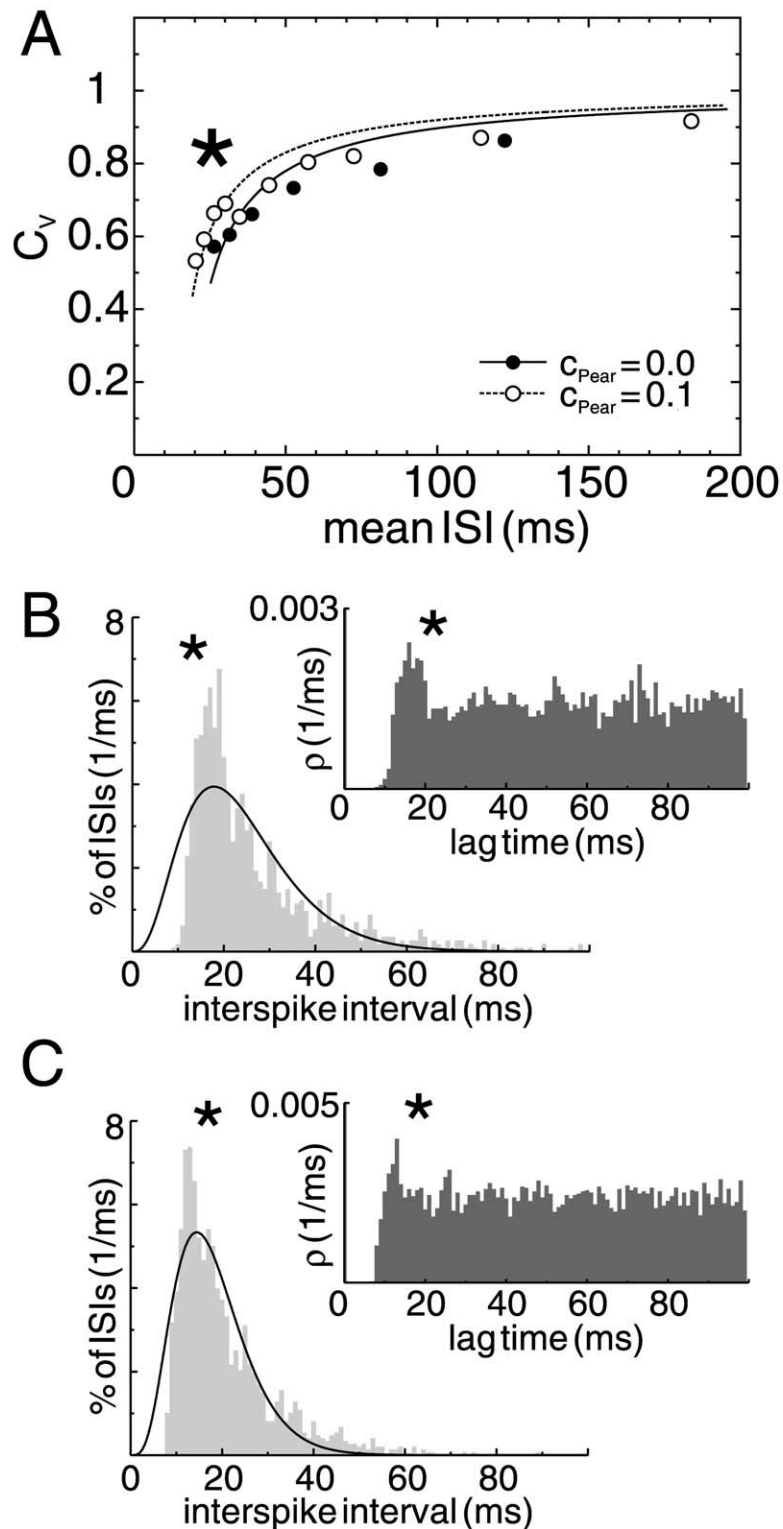


Fig. 7. Irregular firing activity under unbalanced conditions. (A) The C_v as a function of the mean ISI for a fixed inhibitory synaptic release frequency of $\nu_{\text{inh}} = 5.5$ Hz but different excitatory frequencies for two background correlations (zero correlation and correlation corresponding to Pearson correlation coefficient approximately 0.1). Although the C_v under these strongly unbalanced conditions fits well with the behavior expected from Poisson-type activity, the ISIH and autocorrelograms for firing at around 50 Hz (star in A; B shows the results for zero correlation, C for high correlation) depart from the ideal Poisson-type behavior (stars). Both autocorrelograms indicate a preferred ISI of length equal to the effective membrane refractory periods (see fits in A). Fits: Eq. 5 with $T_R = 19.6$ ms for $c_{\text{Pear}} = 0.0$ and $T_R = 15.6$ ms for $c_{\text{Pear}} = 0.1$ (A) Eq. 6 with $q = 3$, $r = 0.168 \text{ ms}^{-1}$, $a = 1.046$ (B) and $q = 4$, $r = 0.277 \text{ ms}^{-1}$, $a = 0.986$ (C).

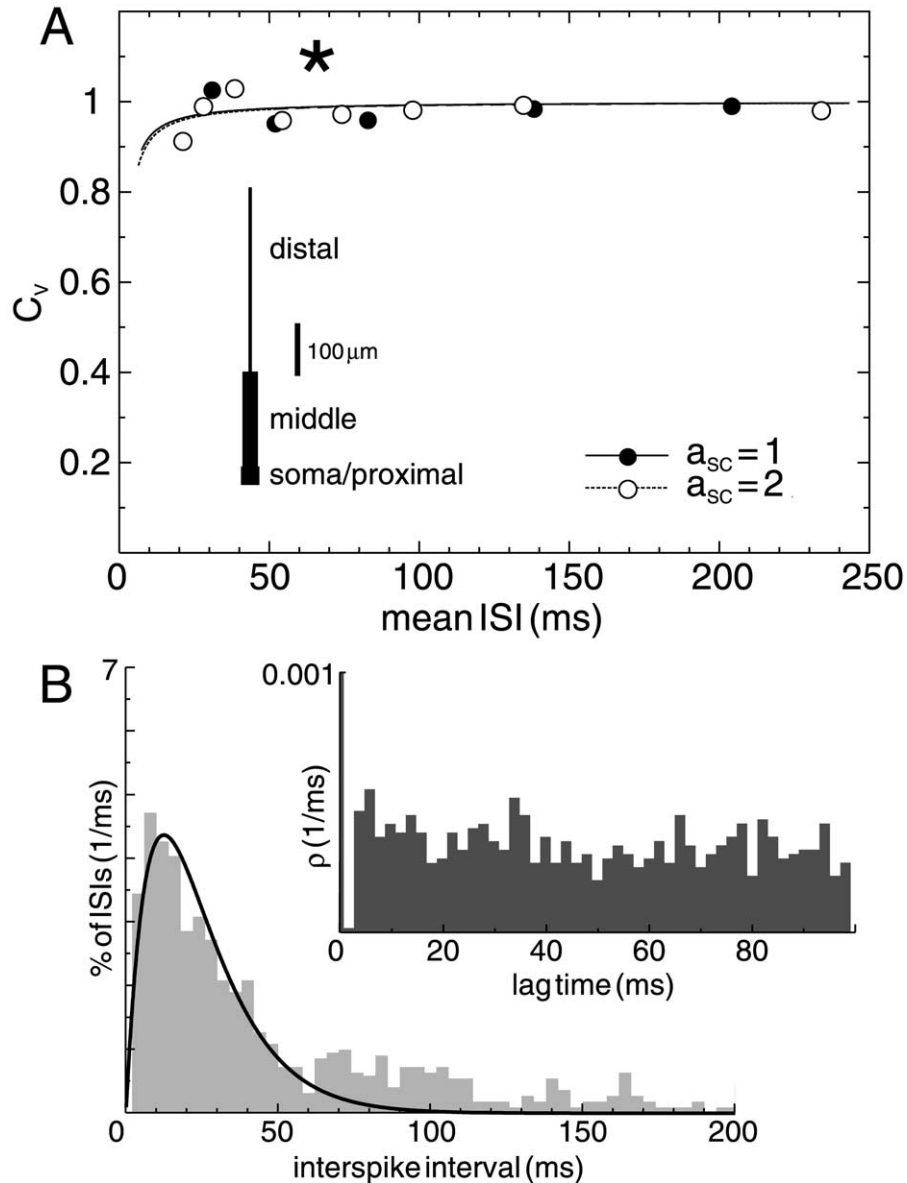


Fig. 8. Irregular firing activity in a three-compartment model (A) The C_v versus mean ISI for two different strength of synaptic conductances (a_{sc} denotes the scaling factor for synaptic conductances with respect to the standard parameter setup; see Experimental Procedures). The inset shows the morphology of the three-compartment model. The star indicates a spontaneous firing rate of about 15 Hz. Fits: Eq. 5 with $T_R = 1.5$ ms for $a_{sc} = 1$ and $T_R = 1.7$ ms for $a_{sc} = 2$. (B) ISIH and autocorrelation (inset) at a firing rate of about 15 Hz (indicated by star in plot A) show that the spontaneous activity resembles nearly that of a Poisson process with small refractory period. Fit: Eq. 6 with $q = 1$, $r = 0.08$ ms $^{-1}$, $a = 1.48$.

that shown in Fig. 6A. For a strong disturbance of the balance between excitation and inhibition, the cell showed a sustained firing at high rates with a preference for an ISI period of 8 ms, which can be viewed as an effective membrane refractory period (see Fig. 9D for an autocorrelation and ISIH at 100 Hz; the deviation from the Poisson structure is indicated by the star). However, for a physiologically realistic spontaneous firing activity below 50 Hz, the ISIs are independent and follow an exponential distribution (see e.g. Fig. 10B).

A high spike variability with C_v values above 0.85 was also obtained when the S.D. of the excitatory and inhibitory synaptic conductances, σ_e and σ_i or the corresponding

time constants τ_e and τ_i were changed independently (Fig. 9B, C). However, in contrast to the aforementioned situation, the ISIHs and autocorrelations had exponential distributions and independence of ISIs in all cases (data not shown). σ_e and σ_i are directly related to the correlation of excitatory and inhibitory synaptic inputs (Destexhe et al., 2001); therefore, these results are consistent with the detailed model. τ_e and τ_i are related to the decay time constants of excitatory and inhibitory synaptic conductances, suggesting a minor impact for these parameters as well.

To address the possible role of a high-conductance state in determining firing variability, we compared conductance-based and current-based models of background ac-

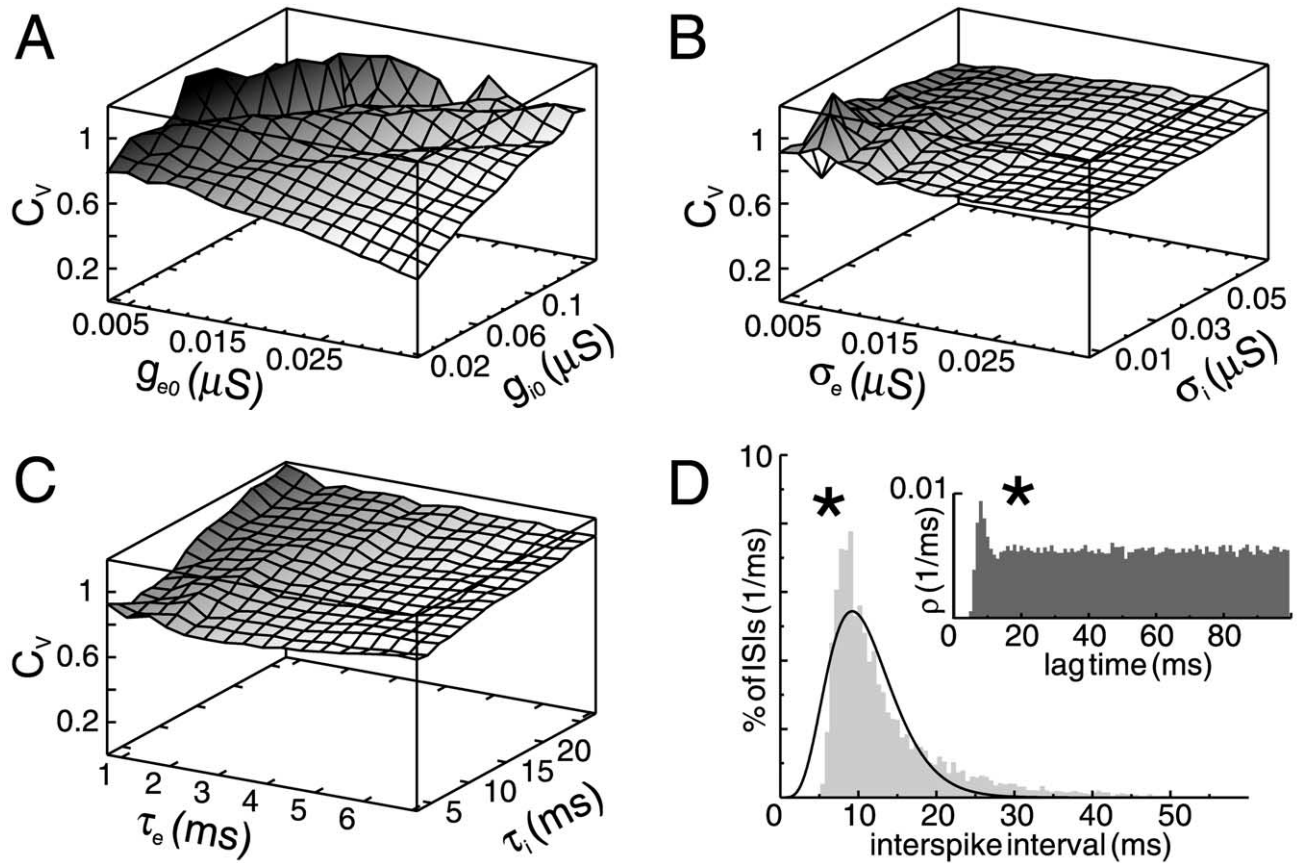


Fig. 9. Irregular firing activity in a single-compartment “point-conductance” model. (A–C) The C_V as a function of the model parameters (see Experimental Procedures; only two parameters were varied at a time while keeping the other parameters fixed at their standard values). (D) ISIH and autocorrelogram (inset) for a very high firing rate around 100 Hz show a deviation from Poisson distribution (stars; model parameters: $g_{e0}=0.035 \mu S$, $g_{i0}=0.573 \mu S$, $\sigma_e=0.012 \mu S$, $\sigma_i=0.0264 \mu S$). Fit: Eq. 6 with $q=5$, $r=0.544 \text{ ms}^{-1}$, $a=0.570$.

tivity. In the fluctuating conductance model shown above, there was a static (DC) conductance (g_{e0} and g_{i0}) with conductance fluctuations. We compared this model with a fluctuating current model, in which noise was injected in the membrane as a DC current with current fluctuations (see Experimental Procedures). We also used two further variations of this model. In one case there was a DC conductance with current fluctuations, and in another case there was a DC current added to fluctuating conductances (see details in Experimental Procedures). We found the highest C_V for the two models having a DC conductance, despite the fact that these models allowed a more effective change in the mean firing rate (Fig. 10A). The C_V was lower for the models with DC current, and lowest for the fluctuating current model with values below 0.6 for firing frequencies above 5 Hz (Fig. 10A).

Marked differences between the discharge activity in models where synaptic background activity was described by conductance or current noise were also revealed when the C_V was investigated as a function of the threshold accessibility (Fig. 5C, left). Here, for a given Δ , the C_V was lowest for the fluctuating-current model and highest for models of high-conductance states (fluctuating-conductance model as well as model with DC conductance). Interestingly, in the latter case there was nearly no change

in the C_V for a broad range of Δ . Contrary, in the fluctuating-current model, the C_V dropped significantly for increasing Δ , i.e. for a decreasing effective distance to firing threshold, as a direct result of the higher discharge rate closer to threshold and the large effective refractory period due to the large membrane time constant in the low-conductance state. In contrast, there was little difference between conductance- and current-based models in the dependence of the mean ISI on the threshold accessibility (Fig. 5C, right).

To test whether the low C_V in the current-based models is due to the small noise time constant τ_{Isyn} , we varied this parameter while adjusting the S.D. of the synaptic current noise (σ_{Isyn}) to yield a constant spontaneous firing frequency of about 15 Hz. τ_{Isyn} values between 2 and 5 ms, which cover the range of time constants of typical fast excitatory and inhibitory synapses, did not lead to an increase in the variability of the output spike train (e.g., $\tau_{\text{Isyn}}=4 \text{ ms}$ yielded $C_V=0.58$). Only for a large increase in the noise time constant we obtained high variability. At the upper limit of the simulated parameter range, $\tau_{\text{Isyn}}=20 \text{ ms}$, the C_V was 0.9.

Another difference between conductance-based and current-based models was also apparent in the ISIHs and autocorrelograms. In models with high conductance, the

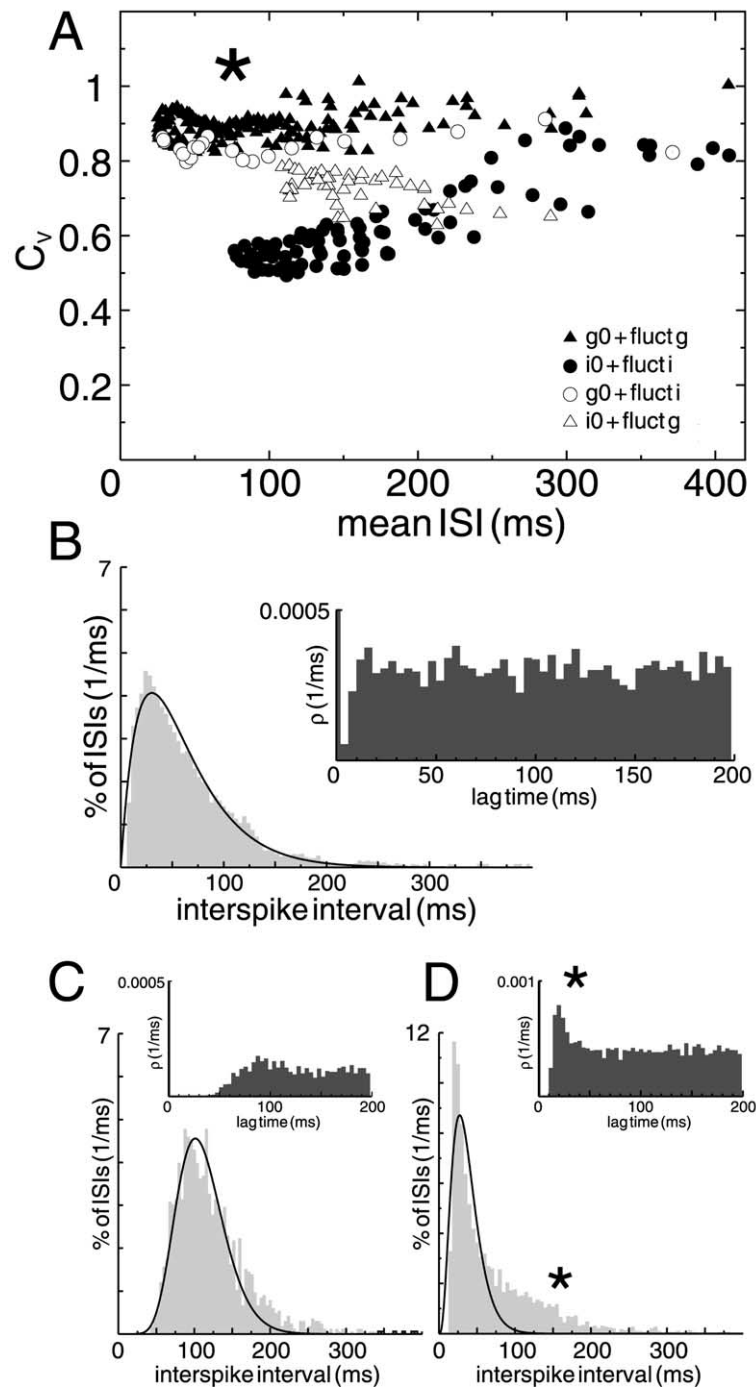


Fig. 10. Evidence that high firing variability is linked to high-conductance states. (A) Comparison of various simplified models of synaptic background activity. In the point-conductance model ($g_0 + \text{fluct } g$), excitatory and inhibitory conductances were changed around a mean according to a Ornstein-Uhlenbeck process, leading to a high C_v around unity. In the fluctuating current model ($i_0 + \text{fluct } i$), random currents around a mean described by an Ornstein-Uhlenbeck process were injected into the cell, leading to a lower variability in the spontaneous discharge activity. In two other models, using a constant current with fluctuating conductance around zero mean ($i_0 + \text{fluct } g$), and a constant conductance with fluctuating current around zero mean ($g_0 + \text{fluct } i$), higher C_v values were obtained, showing that high conductance states account for the high discharge variability. The star indicates a spontaneous firing rate of about 17 Hz. For model parameters and corresponding plots showing the C_v and mean ISI as functions of the threshold accessibility, see Fig. 5C. (B and C) Typical ISI histograms and autocorrelograms (insets) for spontaneous firing rates around 17 Hz (indicated by the star in A) for the fluctuating conductance (model parameters for B: $g_{e0} = 0.0121 \mu\text{S}$, $g_{i0} = 0.0573 \mu\text{S}$, $\sigma_e = 0.015 \mu\text{S}$, $\sigma_i = 0.030 \mu\text{S}$) and fluctuating current model (model parameters for C: $I_{\text{syn}0} = -0.44 \text{ nA}$, $\sigma_{\text{syn}} = 0.36 \text{ nA}$, $\tau_{\text{syn}} = 2 \text{ ms}$). (D) ISI histograms and autocorrelograms (insets) for spontaneous firing rates around 15 Hz for the fluctuating current model with long noise time constant ($I_{\text{syn}0} = -0.44 \text{ nA}$, $\sigma_{\text{syn}} = 0.26 \text{ nA}$, $\tau_{\text{syn}} = 20 \text{ ms}$). The C_v was 0.9, but there is a clear deviation from a Poisson process (indicated by the stars). Fits: Eq. 6 with $q=1$, $r=0.033 \text{ ms}^{-1}$, $a=3.332$ (B), $q=11$, $r=0.108 \text{ ms}^{-1}$, $a=3.515$ (C) and $q=3$, $r=0.11 \text{ ms}^{-1}$, $a=3.53$ (D).

output spike train clearly showed the behavior of a Poisson process, with gamma-distributed and independent ISIs, and a refractory period of about 8 ms (Fig. 10B). On the other hand, the fluctuating-current models deviate from this behavior (Fig. 10C, D). For small τ_{Isyn} of 2 ms we observed a much larger depletion, pointing towards an effective refractory period of about 40 ms. The cell fired preferably with an ISI around 90 ms (Fig. 10C). For large τ_{Isyn} of 20 ms, both the ISIH and the autocorrelogram show a clear deviation from a gamma distribution (Fig. 10D, stars), indicating that the high C_V is not the result of an independent Poisson process, but rather that of an increased occurrence of spike bursts (doublets).

These findings may explain the difference in the C_V value in conductance-based and current-based models. The high-conductance state caused by the ongoing synaptic background activity leads to a marked decrease of the effective membrane time constant, which in turn translates the synaptic background activity into a cellular response with only minimal changes of its Poisson structure. On the other hand, current noise does not lead to a decrease in the membrane time constant, thus causing a severe filtering of short ISIs, which results in a decrease of the variability of the cellular response. In some cases, high C_V can be obtained in current-based models due to an increased occurrence of spike bursts.

DISCUSSION

In this paper we have investigated the spike statistics of spontaneously discharging non-bursting cortical neurons by using both detailed and simplified biophysical models of neocortical pyramidal neurons in the presence of excitatory and inhibitory synaptic background activity. The distributed background activity was adjusted to electrophysiological measurements in cat parietal cortex *in vivo* (Paré et al., 1998; Destexhe and Paré, 1999). We investigated how spike statistics and discharge variability are influenced by various parameters of the background activity. We found that neither its strength (quantal conductance, release rates) nor the balance between excitation and inhibition are stand-alone factors determining a high C_V for physiologically relevant firing rates. We rather found that highly variable ($C_V > 0.8$) Poisson-distributed discharges can be evidenced as a stable qualitative property for a broad parameter range. Provided the neuron was within the limits of explored parameters (e.g. ion channel kinetics and distribution, membrane excitability, morphology) and parameter ranges, we failed to find significant effects of changes on the irregularity of spiking over that expected from a renewal process with a (effective) refractory period.

Intracellular measurements showed that the synaptic background activity present *in vivo* creates a high-conductance state with low input resistance (Matsumura et al., 1988; Baranyi et al., 1993; Contreras et al., 1996; Paré et al., 1998), and therefore of fast membrane time constant. Another prominent feature of *in vivo* recordings is the presence of high-amplitude (σ_V between 2 and 6 mV) voltage fluctuations (Azouz and Gray, 1999; Destexhe and

Paré, 1999; Lampl et al., 1999). Including these characteristics in both detailed (morphologically reconstructed) and simplified (single-compartment) models, led to high C_V values for all models that had a high-conductance component. We therefore propose that the high-conductance state of cortical neurons is essential for maintaining an irregular firing activity in neurons receiving irregular synaptic inputs.

The main support for this proposition is provided by simplified models, in which it was possible to manipulate the excitatory and inhibitory conductances of background activity, and explore their parameter space in detail. We mapped the physiologically meaningful regions of parameters producing (a) highly irregular spontaneous discharges ($C_V > 0.8$); (b) spontaneous firing rates between 5 and 20 Hz; (c) Poisson-distributed ISI intervals; (d) input resistance and voltage fluctuations consistent with *in vivo* estimates. We also compared fluctuating conductance models with fluctuating current models of equivalent voltage fluctuations, but with high input resistance. The latter type is often used to represent synaptic background activity in models (Bugmann et al., 1997; Sakai et al., 1999; Shinomoto et al., 1999; Svirskis and Rinzel, 2000) or in experiments (Holt et al., 1996; Hunter et al., 1998; Stevens and Zador, 1998). However we found here that current-based models lead to a more regular firing (C_V approximately 0.6 for 5–20 Hz firing frequencies) compared to conductance-based models. Intermediate models (high mean conductance with current fluctuations, or mean current with conductance fluctuations) displayed the highest C_V when the high-conductance component was present. This analysis indicates that the most robust way to obtain irregular firing consistent with *in vivo* estimates is to use neuron models in a high-conductance state.

These findings are not in conflict with recent results which outlined that the Ornstein-Uhlenbeck process does not reproduce cortical spiking statistics (Shinomoto et al., 1999). The latter model consisted in white noise injected directly as a current to the membrane, and is therefore equivalent to fluctuating current models. Injection of current as colored noise (Brunel et al., 2001), however, may lead to high C_V , although not with Poisson statistics and only for particular values of the noise time constant (Fig. 10D).

Although the high discharge variability reported here is in accordance with previous conductance-based models, some of our conclusions depart from that of earlier contributions. In the single compartment Hodgkin-Huxley type model of cortical neurons investigated by Bell et al. (1995), a number of cellular and synaptic input parameters were identified which, if correctly combined, yield a balanced or “sensitive” neuronal state. Only in this state, which was characterized by a narrow parameter regime, the cell converted Poisson synaptic inputs into irregular output spike trains. This fine tuning causes the cell to operate close to the threshold for firing, which in turn leads to an input (noise)-driven cellular response. In addition, these authors showed an increase in the variability for stronger inputs. In this case, there was a net decrease of the membrane time

constant, which was identified as the cause of the irregularity (Bell et al., 1995). This is consistent with the necessity of a high-conductance state, as we report here, but the fine tuning required in the above study contrasts with the high robustness that we report here.

A single-compartment model with Hodgkin-Huxley type Na^+ and K^+ currents of hippocampal interneurons subject to Gaussian current noise and Poisson-distributed conductance noise was investigated in Tiesinga and José (1999). For Poisson-distributed inputs, these authors report a net increase in the C_V for fixed mean ISIs for increasing noise variance, and a shift of the C_V versus mean ISI to lower mean ISIs for increasing noise average. However, noise average and variance were quantified in terms of the net synaptic current, leaving a direct link between synaptic conductance and spiking statistics open.

The impact of correlation in the synaptic background on the neuronal response was also investigated by Salinas and Sejnowski (2000) using a conductance-based integrate-and-fire neuron. The authors conclude, in accordance with our findings, that the variability of the neuronal response in an intact microcircuit is mostly determined by the variability of its inputs. In addition, they showed that using a smaller time constant (similar to that found in a high-conductance state) leads to higher C_V values, which is also in agreement with our findings. They also reported a decrease in the variability for an increase in the effective refractory period (relative to the time scale of changes in the postsynaptic conductances) caused by smaller synaptic time constants and larger maximal synaptic conductances. These results hold for a “balanced” model. However, a marked decrease of the C_V was obtained when the “balanced” model was replaced by an “unbalanced” one. Although the sensitivity to the balance in the synaptic inputs was not investigated in detail, the model suggests a peak in the C_V only for a narrow parameter range (see also Bell et al., 1995). The reported C_V values of 1.5 for firing rates of 75 Hz were markedly higher than that found here, presumably because of the occurrence of bursts and significant deviations from the Poisson distribution, as we found here for high firing rates (Figs. 6C, 7, 9D).

Finally, to characterize how fluctuations impact on the discharge variability, we represented the C_V as a function of a measure of “threshold accessibility” Δ . This measure revealed differences between low-conductance and high-conductance states. In low-conductance states, the C_V was dependent on Δ (see Fig. 5C, black dots), consistent with integrate-and-fire models (see e.g. Troyer and Miller, 1997). On the other hand, for high-conductance states, the C_V was mostly independent of threshold accessibility, which is in overall agreement with our main finding, namely that the high discharge variability is highly robust to the details of the model, provided it is operating in a high-conductance state.

In conclusion, in all models examined here, including detailed compartmental models and simplified point neurons, the genesis of highly variable discharges ($C_V > 0.8$ and Poisson-distributed) by membrane-potential fluctuations was highly robust only in high-conductance states.

This relation between high-conductance states and the variability of discharges should be further investigated by future models and dynamic-clamp experiments.

Acknowledgements—Research supported by CNRS and the National Institutes of Health (R01-NS37711).

REFERENCES

- Azouz R, Gray C (1999) Cellular mechanisms contributing to response variability of cortical neurons *in vivo*. *J Neurosci* 19:2209–2223.
- Baranyi A, Szenté MB, Woody CD (1993) Electrophysiological characterization of different types of neurons recorded *in vivo* in the motor cortex of the cat: II. Membrane parameters, action potentials, current-induced voltage responses and electrotonic structures. *J Neurophysiol* 69:1865–1879.
- Bell A, Mainen ZF, Tsodyks M, Sejnowski TJ (1995) “Balancing” of conductances may explain irregular cortical spiking. Tech Report INC-9502. San Diego: The Salk Institute.
- Borg-Graham LJ, Monier C, Frégnac Y (1998) Visual input evokes transient and strong shunting inhibition in visual cortical neurons. *Nature* 393:369–373.
- Brunel N, Chance FS, Fourcaud N, Abbott LF (2001) Effects of synaptic noise and filtering on the frequency response of spiking neurons. *Phys Rev Lett* 86:2186–2189.
- Bugmann G (1995) Controlling the irregularity of spike trains. Research Report NRG-95-04. School of Computing, University of Plymouth, Plymouth, UK.
- Bugmann G, Christodoulou C, Taylor JG (1997) Role of temporal integration and fluctuation detection in the highly irregular firing of a leaky integrator neuron model with partial reset. *Neural Computation* 9:985–1000.
- Burns BD, Webb AC (1976) The spontaneous activity of neurons in the cat’s visual cortex. *Proc R Soc Lond B Biol Sci* 194:211–223.
- Christodoulou C, Bugmann G (2000) Near Poisson-type firing produced by concurrent excitation and inhibition. *Biosystems* 58:41–48.
- Christodoulou C, Bugmann G (2001) Coefficient of variation vs. mean interspike interval curves: what do they tell us about the brain? *Neurocomputing* 38–40:1141–1149.
- Contreras D, Destexhe A, Steriade M (1997) Intracellular and computational characterization of the intracortical inhibitory control of synchronized thalamic inputs *in vivo*. *J Neurophysiol* 78:335–350.
- Contreras D, Timofeev I, Steriade M (1996) Mechanisms of long lasting hyperpolarizations underlying slow sleep oscillations in cat corticothalamic networks. *J Physiol* 494:251–264.
- Cragg BG (1967) The density of synapses and neurons in the motor and visual areas of the cerebral cortex. *J Anat* 101:639–654.
- Dean A (1981) The variability of discharge of simple cells in the cat striate cortex. *Exp Brain Res* 44:437–440.
- DeFelipe J, Fariñas I (1992) The pyramidal neuron of the cerebral cortex: morphological and chemical characteristics of the synaptic inputs. *Prog Neurobiol* 39:563–607.
- Destexhe A (2001) Simplified models of neocortical pyramidal cells preserving somatodendritic voltage attenuation. *Neurocomputing* 38:167–173.
- Destexhe A, Rudolph M, Fellous J-M, Sejnowski TJ (2001) Fluctuating synaptic conductances recreate *in vivo*-like activity in neocortical neurons. *Neuroscience* 107:13–24.
- Destexhe A, Mainen ZF, Sejnowski TJ (1998) Kinetic models of synaptic transmission In: *Methods in neuronal modeling* (Koch C, Segev I, eds), pp 1–26. Cambridge, MA: MIT Press.
- Destexhe A, Paré D (1999) Impact of network activity on the integrative properties of neocortical pyramidal neurons *in vivo*. *J Neurophysiol* 81:1531–1547.
- Evarts EV (1964) Temporal patterns of discharge of pyramidal tract neurons during sleep and waking in the monkey. *J Neurophysiol* 27:152–171.

- Feng J, Brown D (1998) Impact of temporal variation and the balance between excitation and inhibition on the output of the perfect integrate-and-fire model. *Biol Cybern* 78:369–376.
- Feng J, Brown D (1999) Coefficient of variation of interspike intervals greater than 0: how and when? *Biol Cybern* 80:291–297.
- Feng J, Brown D (2000) Impact of correlated inputs on the output of the integrate-and-fire model. *Neural Computation* 12:671–692.
- French CR, Sah P, Buckett KJ, Gage PW (1990) A voltage-dependent persistent sodium current in mammalian hippocampal neurons. *J Gen Physiol* 95:1139–1157.
- Gillespie DT (1996) The mathematics of Brownian motion and Johnson noise. *Am J Phys* 64:225–240.
- Gruner JE, Hirsch JC, Sotelo C (1974) Ultrastructural features of the isolated suprasylvian gyrus. *J Comp Neurol* 154:1–27.
- Gutkin BS, Ermentrout GB (1998) Dynamics of membrane excitability determine interspike interval variability: a link between spike generation mechanisms and cortical spike train statistics. *Neural Computation* 10:1047–1065.
- Hansel D, Sompolinsky H (1996) Chaos and synchrony in a model of a hypercolumn in visual cortex. *J Computational Neurosci* 3:7–34.
- Hines ML, Carnevale NT (1997) The NEURON simulation environment. *Neural Comput* 9:1179–1209.
- Hö N, Destexhe A (2000) Synaptic background activity enhances the responsiveness of neocortical pyramidal neurons. *J Neurophysiol* 84:1488–1496.
- Hodgkin AL, Huxley AF (1952) A quantitative description of membrane current and its application to conduction and excitation in nerve. *J Physiol* 117:500–544.
- Holt GR, Softky WR, Koch C, Douglas RJ (1996) Comparison of discharge variability in vitro and in vivo in cat visual cortex neurons. *J Neurophysiol* 75:1806–1814.
- Holmes WR, Woody CD (1989) Effects of uniform and non-uniform synaptic “activation-distributions” on the cable properties of modeled cortical pyramidal neurons. *Brain Res* 505:12–22.
- Hubel D (1959) Single-unit activity in striate cortex of unrestrained cats. *J Physiol* 147:226–238.
- Huguenard JR, Hamill OP, Prince DA (1988) Developmental changes in nA^+ conductances in rat neocortical neurons: appearance of a slow inactivating component. *J Neurophysiol* 59:778–795.
- Huguenard JR, McCormick DA (1992) Simulation of the currents involved in rhythmic oscillations in thalamic relay neurons. *J Neurophysiol* 68:1373–1383.
- Hunter JD, Milton JG, Thomas PJ, Cowan JD (1998) Resonance effect for neural spike time reliability. *J Neurophysiol* 80:1427–1438.
- König P, Engel AK, Singer W (1996) Integrator or coincidence detector? The role of cortical neurons revisited. *Trends Neurosci* 19:130–137.
- Lampl I, Reichova I, Ferster D (1999) Synchronous membrane potential fluctuations in neurons of the cat visual cortex. *Neuron* 22:361–374.
- Larkman AU (1991) Dendritic morphology of pyramidal neurons of the visual cortex of the rat: III. Spine distributions. *J Comp Neurol* 306:332–343.
- Lin JK, Pawelzik K, Ernst U, Sejnowski T (1998) Irregular synchronous activity in stochastically-coupled networks of integrate-and-fire neurons. *Network Computation Neural Syst* 9:333–344.
- Lytton W (1996) Optimizing synaptic conductance calculation for network simulations. *Neural Computation* 8:501–509.
- Magee JC, Johnston D (1995) Characterization of single voltage-gated sodium and calcium channels in the apical dendrites of rat CA1 pyramidal neurons. *J Physiol* 487:67–90.
- Matsumura M, Cope T, Fetz EE (1988) Sustained excitatory synaptic input to motor cortex neurons in awake animals revealed by intracellular recording of membrane potentials. *Exp Brain Res* 70:463–469.
- McCormick DA, Huguenard JR (1992) A model of the electrophysiological properties of thalamocortical relay neurons. *J Neurophysiol* 68:1384–1400.
- Migliore M, Hoffman DA, Magee JC, Johnston D (1999) Role of an A-type K^+ conductance in the back-propagation of action potentials in the dendrites of hippocampal pyramidal neurons. *J Computational Neurosci* 7:5–15.
- Noda H, Adey R (1970) Firing variability in cat association cortex during sleep and wakefulness. *Brain Res* 18:513–526.
- Nowak LG, Sanchez-Vives MV, McCormick DA (1997) Influence of low and high frequency inputs on spike timing in visual cortical neurons. *Cereb Cortex* 7:487–501.
- Paré D, Shink E, Gaudreau H, Destexhe A, Lang EJ (1998) Impact of spontaneous synaptic activity on the resting properties of cat neocortical neurons *in vivo*. *J Neurophysiol* 79:1450–1460.
- Rudolph M, Destexhe A (2001) Do neocortical pyramidal neurons display stochastic resonance? *J Computational Neurosci* 11:19–34.
- Rudolph M, Destexhe A (2002) Point-conductance models of cortical neurons with high discharge variability. *Neurocomputing* 44–46:147–152.
- Sakai Y, Funahashi S, Shinomoto S (1999) Temporally correlated inputs to leaky integrate-and-fire models can reproduce spiking statistics of cortical neurons. *Neural Networks* 12:1181–1190.
- Salinas E, Sejnowski TJ (2000) Impact of correlated synaptic input on output firing rate and variability in simple neuronal models. *J Neurosci* 20:6193–6209.
- Salinas E, Sejnowski TJ (2001) Correlated neuronal activity and the flow of neural information. *Nat Rev Neurosci* 2:539–550.
- Shadlen MN, Newsome WT (1994) Noise, neural codes and cortical organization. *Curr Opin Neurobiol* 4:569–579.
- Shadlen MN, Newsome WT (1998) The variable discharge of cortical neurons: implications for connectivity, computation, and information coding. *J Neurosci* 18:3870–3896.
- Shinomoto S, Sakai Y, Funahashi S (1999) The Ornstein-Uhlenbeck process does not reproduce spiking statistics of neurons in prefrontal cortex. *Neural Computation* 11:935–951.
- Softky WR, Koch C (1993) The highly irregular firing of cortical cells is inconsistent with temporal integration of random EPSPs. *J Neurosci* 13:334–350.
- Smith DR, Smith GK (1965) A statistical analysis of the continuous activity of single cortical neurons in the cat unanesthetized isolated forebrain. *Biophys J* 5:47–74.
- Steriade M (1978) Cortical long-axoned cells and putative interneurons during the sleep-waking cycle. *Behav Brain Sci* 3:465–514.
- Steriade M, Timofeev I, Grenier F (2001) Natural waking and sleep states: a view from inside neocortical neurons. *J Neurophysiol* 85:1969–1985.
- Stevens CF, Zador AM (1998) Input synchrony and the irregular firing of cortical neurons. *Nature Neurosci* 1:210–217.
- Svirskis G, Rinzel (2000) Influence of temporal correlation of synaptic input on the rate and variability of firing in neurons. *Biophys J* 79:629–637.
- Szentagothai J (1965) The use of degeneration in the investigation of short neuronal connections In: *Progress in brain research* 14 (Singer M, Shade JP, eds), pp 1–32. Amsterdam: Elsevier.
- Tiesinga PHE, José JV (1999) Spiking statistics in noisy hippocampal interneurons. *Neurocomputing* 26–27:299–304.
- Tiesinga PHE, José JV, Sejnowski TJ (2000) Comparison of current-driven and conductance-driven neocortical model neurons with Hodgkin-Huxley voltage-gated channels. *Phys Rev* 62:8413–8419.
- Tolhurst DJ, Movshon JA, Dean AF (1983) The statistical reliability of signals in single neurons in cat and monkey visual cortex. *Vision Res* 23:775–785.
- Traub RD, Miles R, 1991. *Neuronal networks of the hippocampus*. Cambridge, UK: Cambridge University Press.
- Troyer TW, Miller KD (1997) Physiological gain leads to high ISI

- variability in a simple model of a cortical regular spiking cell. *Neural Computation* 9:971–983.
- Uhlenbeck GE, Ornstein LS (1930) On the theory of Brownian motion. *Phys Rev* 36:823–841.
- Usher M, Stemmler M, Koch C, Olami Z (1994) Network amplification of local fluctuations causes high spike rate variability, fractal firing patterns and oscillatory local field potentials. *Neural Computation* 6:795–836.
- White EL (1989) *Cortical circuits*. Boston: Birkhäuser.
- Yamada WM, Koch C, Adams PR (1989) Multiple channels and calcium dynamics. In: *Methods in neuronal modeling* (Koch C, Segev I, eds) pp. 137–170. Cambridge, MA: MIT Press.

(Accepted 18 January 2003)